Adaptive Radiation Therapy for Head and Neck Cancer

Master Thesis
Rikke Busch Eiland

05-March- 2012

Technical University of Denmark
Department of Informatics and Mathematical Modelling
University of Copenhagen
Faculty of Health Science
Copenhagen University Hospital
Department of Radiation Oncology - Herlev Hospital

Technical University of Denmark
Informatics and Mathematical Modelling
Building 321, DK-2800 Kongens Lyngby, Denmark
Phone +45 45253351, Fax +45 45882673
reception@imm.dtu.dk
www.imm.dtu.dk IMM-Master Thesis -2012

Adaptive radiation therapy for head and neck cancer

Author:
Rikke Busch Eiland

Supervisors:
Rasmus R. Paulsen, associate professor at the Section for Image Analysis and Computer Graphics (IACG) at the Department for Mathematical Modelling (IMM) at the Technical University of Denmark (DTU).

Claus Behrens, PhD.
Department of Radiation Oncology,
Copenhagen University Hospital - Herlev

David Sjöström, PhD.
Department of Radiation Oncology,
Copenhagen University Hospital - Herlev

Eva Samsø, PhD.
Department of Radiation Oncology,
Copenhagen University Hospital - Herlev

Master Thesis conducted: 09/05/11- 03/05/12

ECTS points: 30

Edition: 1. Edition

Comments: This thesis is part of the requirements to achieve Master of Science in Engineering (M.Sc.) at Technical University of Denmark and Copenhagen University

Abstract

Purpose
Anatomical changes can occur during radiation therapy of head and neck cancer patients. This can lead to discrepancies between planned and delivered dose. Adaptive radiation therapy has the potential to overcome this using deformable image registration (DIR). The purpose of this study was to evaluate the performance of a DIR algorithm using geometric and dosimetric measures.

Materials and Methods
Seven patients treated with IMRT were included in this study, each with a planning- and midterm CT (pCT, ReCT) as well as a CBCT acquired at the same time as the ReCT. ReCT served as ground truth for evaluation of the DIR. A deformed CT (dCT) with structures was created by deforming the pCT and associating manually delineated structures to the CBCT. A commercial software package using a Demons type of DIR algorithm (SmartAdapt, Varian medical Systems v.11.0) was used. The geometrical comparisons were based on structures of the dCT, and manually delineated structures on the ReCT.
In the treatment planning system (Eclipse, Varian Medical Systems, v. 10.0) the initial treatment plan was transferred to the dCT and the ReCT and the dose recalculated.

Results
Geometrical similarity between target structures of dCT and ReCT was found, especially with respect to PTV and CTV. Small variation was observed for the Parotid glands. The spinal cord obtained poor geometrical similarity.
Non-significant difference between the dosimetric outcome of dCT- and ReCT-based dose calculation was observed. Investigating the possibility for CBCT-based dose calculation revealed no significant difference when comparing to dose

based on ReCT.

Conclusion
Similarity was found between deformed and manually delineated structures of dCT and ReCT. An exception was the spinal cord, indicating that the DIR is not usable for this organ. Large similarity in dose provided for the target structures was found for dCT- and ReCT-based dose calculation. Generally, the DIR between pCT and CBCT represent a feasible tool for adaptive radiation therapy, with regard to target structures and the parotid glands.

Resume

Formål
Ved strålebehandling af patienter med hoved-hals cancer kan anatomiske ændringer opstå som følge af bl.a. tumor svind og vægttab. Dette kan medføre en forskel mellem den planlagte og givne stråledosis. Adaptiv strålebehandling har potentiale til løse dette problem ved benyttelse af deform billederegistrering (DIR). Formålet med dette studie var at evaluere resultater opnået ved brug af en DIR algoritme. Evalueringen er baseret på geometriske og dosimetrisk mål.

Materialer og metoder
Syv patienter behandlet med IMRT blev inkluderet i dette studie. Hver patient havde en planlægnings-og midtvejs CT (pCT, ReCT). Ligeledes var en cone beam CT opsamlet samme dag som ReCT tilgængelig. ReCT blev defineret som *ground truth* og brugt til evaluering af DIRen. En deform CT (dCT_{CBCT}) med strukturer blev dannet ved at deformere pCT til CBCT. Deformeringen blev udført ved hjælp af kommerciel software (SmartAdapt, Varian Medical Systems v.11.0). Deformeringen opnået i SmartAdapt bygger på en Demon algoritme. Den geometriske sammenligning blev baseret på deformerede strukturer på dCT og manuelt optegnede strukturer på ReCT.
I dosis planlægningssystemet (Eclipse, Varian Medical Systems, v. 10,0) blev den oprindelige behandling plan overført til dCT og ReCT og dosis genberegnet.

Resultater
Ved sammenligning af deformerede stukture opnået ved brug af CBCT og manuelt optegnede strukturer på ReCT, blev der fundet stor lighed mellem target strukturer, specielt CTV og PTV. Der blev ligeledes fundet en lighed mellem parotis kirtel strukturere for RecT og dCT, dog med nogen variation. Begrænset geometrisk lighed blev fundet for rygmarvsstrukturen.

Ved sosimetrisk sammenligning blev der fundet lille forskel mellem dCT- og ReCT-baserede dosisberegning. CBCT-baserede dosisberegning viste ingen signifikant forskel til dosis udregnet på RECT.

Konklusion
Stor lighed mellem deformerede og manuelt optegnede strukturer blev fundet, dog med undtagelse af rygmarvsstukturen.
Dosis til target-strukturer blev fundet af samme størrelse for dCT_{CBCT}- og ReCT-baseret dosisberegning. Overordnet repræsenterer deform registrering mellem pCT og CBCT et brugbart værktøj for adaptiv strålebehandling, med hensyn til target strukturer og parotis kirtlerne.

Preface

This master thesis was produced at the department of Informatics and Mathematical Modelling at the Technical University of Denmark and the Department of Oncology at Copenhagen University Hospital - Herlev Hospital. The thesis has been produced from September 5th 2011 to March 5th 2012, and account for 30 ECTS point.

Lyngby, 05-March-2012

Rikke Busch Eiland

Acknowledgements

I wish to thank my supervisors, Rasmus Paulsen, Eva Samsø and David Sjöström for their guidance and support throughout this work. A special thank goes to my supervisor Claus Behrens for his great help, encouragement and constructive criticism. I would also like to thank for the opportunity to conduct my master thesis at the Department of Radiation Oncology at Herlev Hospital. Additionally I thank Christian Maare for making comparison to a new CT scan possible and for confirmation of the collected data. I thank Benjamin Hass, Varian®, for help provided to understanding of the software used in this thesis. I would also like to thank additional staff on the Department of Radiation oncology at Herlev hospital for help and guidance provided when needed.
Finally, I would like to thank my family and friends for their support throughout this project.

Papers included in the thesis

A R.B. Eiland, C.F. Behrens, D. Sjöström, C. Maare, R.R. Paulsen, E. Samsoe. Dosimetric- and geometric evaluation of adaptive *H&N* IMRT using deformable image registration. Abstract, Accepted for poster presentation at *ESTRO 31 conference*, 2012.

B R.B. Eiland. Adaptive Radiation Therapy. Poster presentation at *Department for mathematical Modelling (IMM) at DTU*, 2011.

Available in appurtenant appendix.

Contents

List of Figures

List of Tables

List of Abbreviation

Abbreviation	Explanation
AAA	Anisotropic Analytical Algorithm
ANOVA	ANalysis Of Variance
ART	Adaptive Radio Therapy
CBCT	Cone Beam Computed Tomography
CI	Conformity Index
CT	Computed Tomography
CTV	Clinical Target Volume
COM	Center Of Mass shift
DAHANCA	DAnish Head And Neck CAncer group
DEDM	Deformed Electron Density Mapping
dCT_{CBCT}	Deformed Computed Tomography based on CBCT
dCT_{ReCT}	Deformed Computed Tomography based on ReCT
Dex	Dexter (Latin for right)
DICOM	Digital Imaging and COmmunication in Medicine
DIR	Deformable Image Registration
DSC	Dice Similarity Coefficient
DVH	Dose Volume Histogram
FOV	Field Of View
Frac	Fraction
GTV	Gross Target Volume
Gy	Gray (J/kg)
H&N	Head and Neck

Abbreviation	Explanation
HU	Hounsfield Unit
ICRU	International Commission of Radiation Units
IMRT	Intensity modulated Radiation Therapy
IGRT	Image Guided Radiation Therapy
LCF	Lesion Coverage fraction
MLC	MultiLeaf Collimator
MRI	Magnetic Resonance Imaging
MU	Monitor Units
NTOF	Normal Tissue Overdosage Fraction
NTCP	Normal Tissue Complication Probability
OAR	Organs At Risk
OI	Overlap Index
pCT	planning CT
PET	Positron Emission Tomography
PRV	Planning organ at Risk Volume
PTV	Planning Target Volume
QQ-plot	quantile-quantile plot
ReCT	Rescanning CT
ROI	Region Of Interest
RT	Radiation Therapy
RTOG	Radiation Therapy Oncology Group
SD	Standard Deviation
Sin	Sinister (Latin for left)
TCP	Tumour Control Probability
TPS	Treatment Planing System
TRE	Target Registration Error
TV	Treated Volume
VOI	Volume Of Interest

Chapter 1

Introduction

Cancers in the head and neck area are often treated using radiation therapy. This presents certain challenges in sparing adjacent organs from unnecessary irradiation.
When first planning the treatment, computed tomography (CT) scan is used. This allows for manual delineation of the tumour and nearby organs to ensure optimal delivery of the radiation. During the course of treatment, the size of the tumour can change drastically. This can potentially lead to difference between planned- and delivered dose. To overcome this, a new treatment plan based on a new CT, must be implemented [50, 11, 26]. However, this is a very time consuming process involving several health care professionals. As such, a new treatment plan is only made when drastic changes in the anatomy are observed. The decision on whether or not to adapt the treatment plan will be based on a cone beam computed tomography (CBCT) scan. This scan is performed in the treatment room, in connection with an on-going treatment. The quality of a CBCT scan is however poor compared to that of an ordinary CT.
By the use of image analysis it has been possible to make use of CBCT for adaptation of the treatment plans [29, 45, 23]. Special software can be used to perform deformable image registration (DIR) and deform the initial CT (pCT) to match the CBCT. The results will be a set of deformed CT images (dCT_{CBCT}), containing the structural information from the CBCT, depicting the actual anatomy, and the image quality of the initial CT. Manual delineation on the pCT can be deformed to match the new deformed image. Based on the

set of deformed images and structures the hypothesis is that it should be possible to recalculate the original treatment plan thereby adapt the plan to the newly changed anatomy.

The aim of this study is to evaluate the performance of an available DIR using geometric and dosimetric measure.
A commercial software package using a variant of the Demons DIR algorithm (SmartAdapt® Varian Medical Systems, v.11.0) is utilized. A CT acquired at the same time as the CBCT serves as ground truth for the evaluation. By use of the new CT (ReCT) as ground truth it is possible to evaluate if a deformed CT with deformed structures can replace a new CT with manually delineate structures. Geometrical comparison is based on the estimated volumes from the structures on the dCT_{CBCT} and the manually delineated structures on ReCT. Utilizing a treatment planning system (Eclipse®, Varian Medical System v.10.0) the dose distribution is calculated based on the dCT_{CBCT} and ReCT. Figure 1.1 illustrates the four image set used and compared in this thesis.

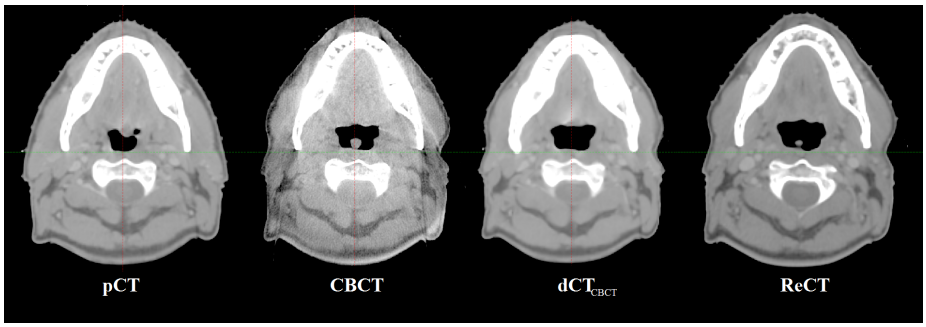

Figure 1.1: Example of the four type of image sets used in this thesis. Patient ID: 136

Chapter 2

Background

In the following chapter the general aspects of radiation therapy will be presented. In Section 2.1, the typical process of treatment planning and delivery in radiation therapy will be described. The modalities used are briefly described in Section 2.3. The reader will also be given a brief introduction to image registration in Section 2.4. Finally the concept of adaptive radiation therapy will be introduced, Section 2.5. Experienced readers can skip this chapter.

2.1 Course of treatment

Typically, cancer in the head and neck area will be discovered by a general practitioner or a dentist. The next step will be a referral to an ear-nose and throat specialist, which again in the case of a positive finding will, refer the patient to an oncological center. The final diagnosis is determined at this facility. Decisions regarding the type of treatment is made by a team of specialists [4]. Radiation can be chosen as part of the treatment and is often combined with chemotherapy since the combination improves the chance of recovery, [49]. This chapter has focus on the course of treatment with regard to the radiotherapy. Figure 2.1 shows the progression of the treatment course.

Figure 2.1: Course of treatment

Planning the treatment

Immobilization

Prior to treatment, a device for patient immobilization must be made. This device used for H&N cancer patients are a thermoplastic mask that is custom made to fit the individual patient (Figure 2.2). The mask will be attached to the treatment table to fixate the patient and serve as head support. The immobilization of the patient is crucial to ensure the accuracy of the treatment [27].

Figure 2.2: Example of a thermoplastic mask for fixation of a head and neck cancer patient, [28]

Image acquisition

Typical image modalities used in radiation therapy are computed tomography (CT), magnetic resonance imaging (MRI) and positron emission tomography (PET). The modalities have different advantages and disadvantages and are often combined to determine the location of tumour and the critical organs. The patient will always receive a CT scan, since this is used for planning of the treatment. The CT must be conducted while the patient is immobilized [27, 40].

Treatment planning

Delineation of the tumour and critical organs are performed on a CT scan called a planning CT (pCT). To assist the delineation, additional modalities are used, as well as clinical evidence obtained by i.a. visual examination of the patient and biopsies. Delineation of the structures will be performed by manually drawing on the slices of the CT. Organs with a clear boundary can be delineated automatic by the use of atlas or model based tools available in the treatment planning system (TPS) [40]. In the H&N area, a lot of high risk organs such as the spinal cord, salivary gland and the optic nerve are present. By delineating the OAR it is possible to design the treatment around these areas and protect them against irradiation [27]. Elaboration of the delineation process is described in Section 2.3.

The beam arrangement is performed by a physicist/dosimetrist, and is the next step in the planning process. Different treatment techniques are used for different kinds of cancers. The treatment technique typically used in H&N cancer is intensity modulated radiation therapy (IMRT). This technique typically uses six beams placed in different angels around the patient. The intensity and shape of the beams are altered during the treatment, with the help of a multi-leaf-collimator (MLC)(Figure 2.3(a) and 2.3(b)) [40].
When the beam geometry has been designed a coarse optimization is performed. This is done prior to calculation of the 3D-dose distribution. The dose calculation is based on different algorithms, all with the intent of predicting the delivered dose to the patient. By the use of the TPS it is possible to optimize the dose distribution. The optimization is based on dose constrains, with respect to the tumour coverage, and minimization of dose to OAR [5]. Different values are used to validate the plan. Depending on the type of tumour, the patient will get a suitable prescribed dose. For H&N cancer patients, the typical dose to tumour will be between 58 and 68 Gy. Every treatment is fractionated, causing the patient to typically receive six fractions a week. One fraction per day in six days, or one fraction per day in five days and two factions one day with a six hours interval [17]. This procedure is used due to a connection between the dose and the fraction of surviving cells [12]. The smaller dose, the larger survival rate of cells. Because as much as the normal tissue needs to survive, the dose is divided into small doses; fractions.

Before any treatment can be given to a patient quality assurance must be conducted. Every dose plan must undergo independent control. This control ensures that the prescribed dose is provided and that satisfactory dose coverage is obtained in every slice of the CT. Likewise is every dose constrains evaluated. Additional, the dose calculation conducted in the primary TPS are recalculated in a secondary TPS. This is performed to ensure the dose calculation in cor-

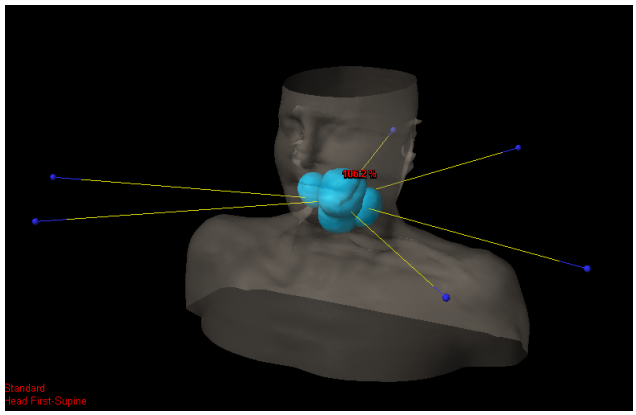

(a) 3D presentation of six fields used for IMRT. Fields are presented as lines. Patient 134

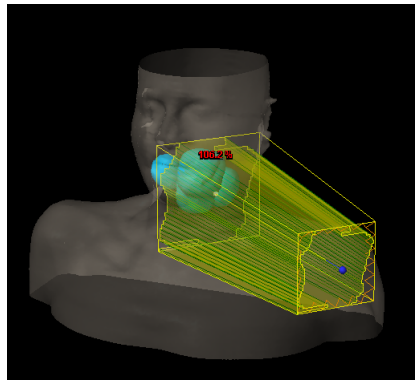

(b) 3D presentation of one field. Fields are presented as a cone depicting the MLC placement for this exact field. Patient 134

Figure 2.3: 3D presentation of fields used for provided at IMRT for H&N patient

rect and uniform dose is provided in every TPS [17]. For every patient selected information regarding provided dose is reported to the Danish Head and Neck Cancer Group (DAHANCA).

Patient treatment

The treatment is delivered to the patient in a treatment room with a medical linear accelerator (linac) (Figure 2.4). It is important that the patient is placed in the same position at every treatment. The patient is therefore placed in the immobilization mask, and lasers provided in the room are used to ensure the positioning and thereby minimize set-up errors. Furthermore the position of the patients head is validated with images in 2- or 3D [32].

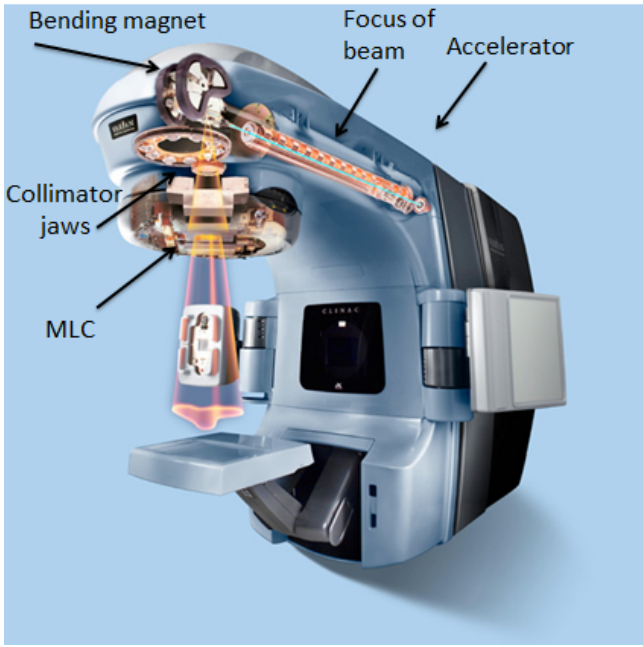

Figure 2.4: Overview of the components of the linac. Modified from [1]

The gantry of the linac rotates around the patient providing a conform X-ray beam towards the target. The linac can produce electron and photon radiation. Electrons are produced in an electron gun and accelerated in an accelerator. A bending magnet, in the upper part of the gantry is the used to bend the electron beam towards the patient. An X-ray beam is produced by directing

the electron beam towards a high-density metal, which slows down the electrons and produces photons. This is similar to the generation of the Bremsstrahlung radiation in X-ray tubes used for medical imaging, but with much higher energy. The beam will need filtering to make it conform, and is shaped with the use of two types of collimators. The collimators are placed in the head of the gantry and consist of jaws and a MLC. The jaws are used to make a rectangular field, and the MLC are used to shape the field (Figure 2.3(b)). The MLC consist of a set of collimator leafs which can slide side by side to make the desired shape of the field [32].

2.2 Image Modalities

In this study images from helical CT, and CBCT will be used. This section presents the two modalities, and discusses the benefits and disadvantages for both.

2.2.0.1 CT and CBCT

When conducting a CT scan, a 3D volume is reconstructed by a large set of X-ray projections obtained from angles around the patient. An X-ray tube rotates around the patient while emitting x-rays that attenuates while passing through the body. The X-ray tube provides a fan shaped beam. During image acquisition of helical CT the couch will be moving. As a result the X-ray tube will move in a helical pattern. The detector system, on the opposite side, will measure the intensity of the attenuated beam, and convert it into an electrical signal. The data is reconstructed into a 3D volume by for example using filtered back projection [6], [12, p. 356].
Each voxel in the reconstructed CT image will represent a Hounsfield unit (HU) value. This value describes the attenuation of X-ray within the voxel.
The average energy of the X-ray beam used in CT image production will be around 70kV. At this energy the dominant interaction to the total attenuation will be Compton scattering. However because the X-ray beam consist of a spectrum of energies, photoelectric effect will also be present (Figure 2.5) [15, p. 148]. Contrast in CT-images will mainly depict the physical properties of tissue influencing the Compton scatter, due to Compton being the most dominant interaction [12, p. 356],[15, p. 154], [32, p. 204]. Compton scatter is influence by, among others, the density, atomic number, as well as the electron density. Hence HU values are derived based on these physical properties [12, p. 356].

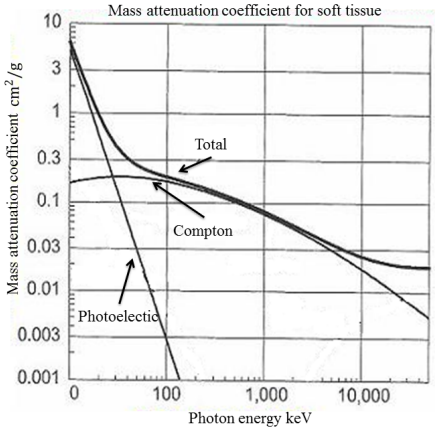

Figure 2.5: Total linear attenuation coefficient for water as a function of energy. Contributors to the total linear attenuation are Compton scattering and photoelectric absorption, which are also displayed. Modified from [2]

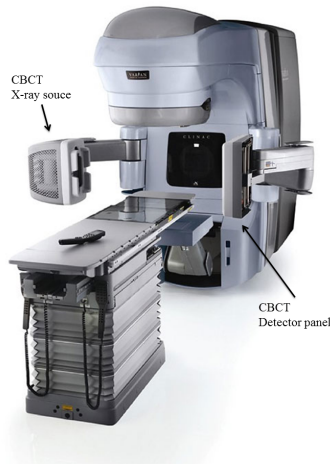

Figure 2.6: Illustration of the CBCT mounted on the treatment unit, modified from [3]

The treatment unit is provided with a CBCT scanner (Figure 2.6). This makes it possible to obtain images under actual treatment conditions. The X-ray beam used in CBCT is cone shaped in contrast to the CT where the beam is fan shaped (Figure 2.7) [18]. A 3D-volume of the patient is acquired with only one rotation of the beam, and lower dose than ordinary CT. Reconstruction is performed with different kinds of cone beam-filtered back projection algorithms. CBCT can be used as a tool for patient set up and adaptive replanning. Because the CBCT is acquired while the patient is on the treatment couch, it will save the patient for a perhaps painful extra CT scan.
There is different benefits and disadvantages by using CBCT images compared to CT images, and these will be discussed below.

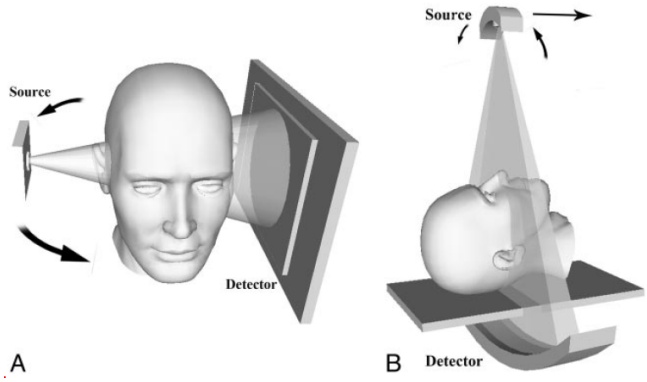

Figure 2.7: Illustration of different beam and detector types. A: Cone Beam B: Fan beam used in CT [38]

2.2.0.2 CBCT vs. CT

The image acquisition is different in the two image modalities. As described above a helical CT requires rotation and translation in the z-direction to obtain data. The CBCT uses a different kind of detectors which makes it possible to obtain a volumetric dataset in only one rotation of the X-ray source. The detectors in a fan-beam will be placed in on array[1], while the detectors in CBCT are placed in a flat-panel (Figure 2.7) [38], [34, p. 20].

A problem with CBCT is increased amount of scatter, which reduces the image

[1] Most clinical CT-scanner will use multi-slice where the CT-scanner acquires multiple slices using multiple arrays of parallel detectors.

quality compared to conventional CT. Scatter is produced in the body during image acquisition when the X-rays is send through the patient. Scatter is of stochastic occurrence and it is not possible to know where it will be produced or end up in advance [38][34, p. 20].
In conventional CT, the X-ray beam and detectors are in a narrow plan. This means that scattered photons fall outside this plan. In CBCT is the beam wide and detector plan big, which makes the possibility of detecting scattered photons together with primary photons larger. Conventional fan beam CT will additional typical have a collimator in front of the detector that only allow scatter from a small axial volume to reach the detector. CBCT do not have this collimator and is thereby allowing scatter from the entire volume to reach the detector. The enlarged amount of scatter allowed in CBCT will reduce the signal-to-noise ratio, leading to a poorer image quality [38].

The amount of scattered radiation will vary depending on different factors, such as the size of radiated volume. A large irradiated volume will produce an enlarged amount of scatter, compared to a smaller volume [34, p. 20].
HU values are based on the attenuation of radiation though the patient. Due to the limitations of CBCT caused by the size of the irradiated volume, and the missing collimator, the detectors will receive falsely information of the attenuated beam, and the HU value will not be correct [35]. It is not yet possible to, easily, come around this problem. Finally, CBCT has a limited scan range in the superior inferior direction. It will therefore not always be possible to image the complete treated volume.

2.3 Volume delineation

Volume delineation is delineation of specific volumes inside the patient (Figure 2.8). The delineation is performed by an oncologist and a radiologist.
The specific volumes which typically considered are:

- GTV - Gross Target Volume
- CTV - Clinical Target Volume
- PTV - Planning Target Volume
- OAR - Organ at Risk
- PRV - Planning organ at Risk Volume

The GTV consists of the verified tumour tissue and positive lymph nodes. Delineation of GTV is often based on different image modalities, e.g. a combination of CT, MRI and PET as well as clinical evidences from visual evaluation and biopsies [39]. The GTV is divided into subtypes, GTV-T to represent the primary tumour and GTV-N to represent lymph node metastases (positive lymph node).

The CTV is the volume containing the GTV and tissue suspected to contain microscopic tumour extensions. These tumour extensions will not be visual on any images. The size of the CTV is a probability assessment based on knowledge of biological and clinical behaviour of the specific tumour type. Knowledge of the surrounding tissue, is also used for the evaluation [31]. Delineation of CTV is based on clinical experience of the physician.

The PTV consists of the CTV with the addition of a margin. The purpose of this margin is to account for changes in the patient set up, or internal movement in the patient as well as the penumbra. The margin ensures that the CTV receives the prescribed dose during each treatment [27, 10].

An OAR is a normal tissue that is sensitive to irradiation. Guidelines concerning the dose constrains to the OAR, are followed in the process of treatment planning. These guidelines include a tolerance level for each type of organ that should not be exceed, see also Section 4.3.2. To further ensure that the dose to the OAR at all times fall within the tolerance level, a margin is set around the volume. This safety margin is called PRV and is, like in PTV, introduced to account for set-up errors and internal organ motion [17, 31].

It is important to remember that all delineations of volumes only represent

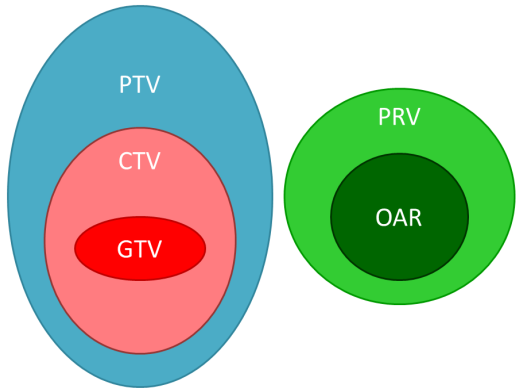

Figure 2.8: Diagram of basic delineation. Inspired from [40]

a snapshot in time. Changes in the anatomy can over a period of time occur and the delineation of a certain volume might not be as representative [31]. The wide interest in adaptive radiation therapy is based on this problematic issue. Several studies, including this, works with different solutions to easily adapt the structures to the actual anatomy of the patient.
Figure 2.9 illustrates an example of delineation performed on a patient. Included in the figure are both target and OAR structures.

2.4 Image registration

Image registration is an important part of radiation treatment and delivery. While delineating structures it might be necessary to use MR images to see the soft tissue differences. To combine the information from the MRI and the CT it is crucial to perform image registration. To secure the patient set-up during treatment images are provided while the patient is on the treatment couch. By registering these images with the ones obtained at the pCT, it will be possible to position the patient correctly. It might also be necessary to obtain images of the patient during the duration of the period to investigate for any significant differences in the anatomy of the patient. When registering two different images, it is possible to observe the changes and investigate if the proposed treatment plan still fulfils the given standards.

When performing image registration, a source and target image is defined. The goal is to transform the source image, to become similar to the target image. This is done by a suitable geometrical transformation [33]. There are two dif-

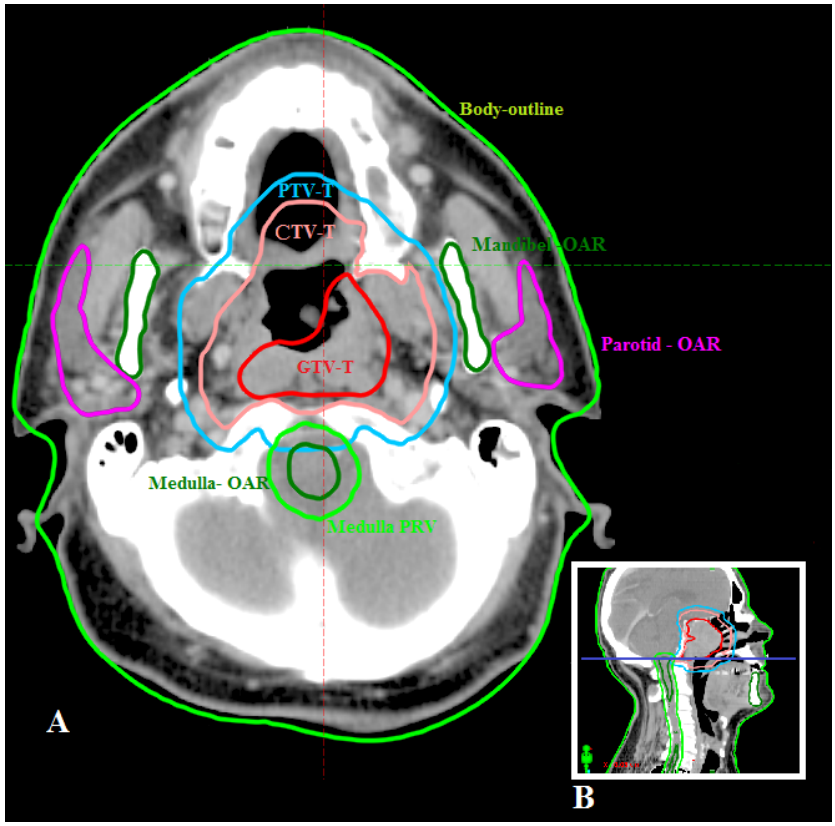

Figure 2.9: Example of definition of volumes on a CT-scan for a head and neck cancer patient. *A* examples of various volumes in the axial plan. *B*: Sagittal view is shown and the blue line depicts the axial plan shown in A. Patient not included in this study

ferent methods for image registration: rigid and non-rigid.
The rigid transformation is used for translation and rotation only. Translation is performed along the x, y and z axis, while rotation consists of pitch, yaw and roll. This gives a total of six parameters [13]. The rigid transformation is used to correct for different patient positions between scans [33].
The non-rigid transformation is used in some cases when the rigid transformation is not sufficient. This is the case if the patient has experienced changes that are not due to set up error. An example could be anatomical changes in the patient. The non-rigid transformation which is typically used in radiation therapy is a deformable image registration (DIR) [42].
The procedure of image registration can be divided into three components [16]:

- Similarity measure: Used to determine how well the images match.
- Transformation model: Specifies how the source image is changed to match the target image.
- Optimization process: Variation of parameters in the transformation model, to maximise the similarity measure.

The type of similarity measure and optimization process used is based on the modalities of the images, and the type of registration.

In this study a rigid registration followed by a DIR is used. The DIR is based on a Demons type of algorithm, which deforms the pCT to match a midterm CBCT. The exact algorithm used in SmartAdpat® is proprietary. A related type of DIR algorithm, have been validated by Wang et al. [48]. A demons type of DIR algorithm was found to perform the best among different DIR strategies by Castadot et al.[13]. Following chapter present a cursory description of a demons type algorithm witch is believed to be similar to the type of Demons algorithm used in the software.

Demons Algorithm

The Demons algorithm is based on intensity similarities of the images and was originally presented by Thirion (1998)[43]. The Demons algorithm is widely used in medical image registration [29]. The Demons algorithm exists in a variety of forms. The variant used in this study is a free form deformation.
In the Demons algorithm the two images which are to be registered are defined as a static and a moving image respectively. The static image will, in this study, be the CBCT image while the moving will be pCT. The basic idea behind the

algorithm is the placement of demons[2]in the static image. The localisations of the demons are based on the gradients of the static image. Every voxel, where the gradient of the static image is different from zero, will be assigned a demon [43]. A displacement between two points in two images with similar intensity is determined. Based on this displacement the demons will apply a force to the moving image. The force and displacement can be viewed as a transformation model. The process is iterative, and every time the demons have applied a force to the points in the moving image, a new displacement will be derived. The process continues until a selected number of iterations have been reached [43].

[2]The concept of demons arises from Maxwell demons. He assumed that a gas of hot and cold particles was placed in a container, separated by a semi-permeable membrane. In this membrane a set of demons were placed. These were able to distinguish between the particles and sort them. This corresponds to a decrease in the entropy which is in contradiction with the second law of thermodynamics. Maxwell solved the paradox by adding the extra amount of entropy generated by the demons [43]

2.5 Adaptive Radiotherapy

The goal of radiation therapy is to enhance tumour control[3] and reduce side effects. In recent years the accuracy of the treatment delivery has been improved, which provides a more conform radiation. As a consequence the treatment plan is sensitive to changes in the patient from day to day. Changes can occur due to set-up errors and anatomical changes. This can lead to incorrect low dosage to tumour and/or too high dose to normal surrounding tissues [26, 22].
Set-up errors can be minimized by rigid patient immobilization and position correction based on X-ray and CBCT images (See Section 2.2.0.1). These procedures are inadequate to account for geometrical errors due to changes of the patient's anatomy. Anatomical changes occur due to e.g. weight loss and tissue shrinkage. OAR close to the tumour can, because of changes in the anatomy, get closer to or even inside the volume treated with high dosage. Neighbouring organs in the H&N area lie very close and even small changes can have consequences for dose to OAR [22].
Barker et al. have found considerable volume reduction of the tumour in H&N during treatment. Additionally they found a shift in the center of mass of the tumour. A high correlation with the amount of tumour loss was found for the parotid glands were also found by Barker et al.[11].
Hansen et al. focuses on the dosimetric impact of anatomical changes and found dose to spinal cord and brain stem to increase during treatment. A decrease in the dose to the tumour was found, which compromises the tumour control [26].

Figure 2.10(a) and 2.10(b) are examples of anatomical changes affecting the OAR. It shows the patient before the treatment has begun and later in the treatment course (week three of treatment). On both scans the volumes of OAR are delineated. The body outline on 2.10(b), reveals that the patient has experienced weight loss and tissue shrinkage during the treatment. Due to the anatomical changes, the delineated volumes of the parotid glands no longer match. The spinal cord, which is encircled by the columna, has not moved noticeable.
Figure 2.11 visualises the target structures for pCT and ReCT. Anatomical changes has occurred, and the original target structures are too large and shifted compared to the new structures. The consequence can be unwanted dose to normal tissue, and compromised tumour control. The examples above illustrates that adaptive radiation therapy is necessary to improve the tumour control and protection of normal tissue.

[3] Tumour control is an expression for correct treatment of tumour. This is obtained by killing of tumour cells.

(a) pCT. Patient ID 138

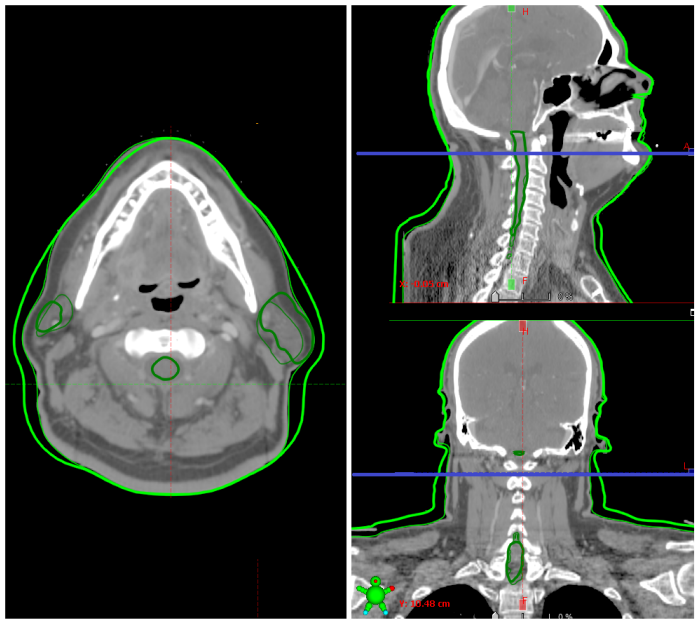

(b) ReCT. Patient ID 138

Figure 2.10: CT scan of patient 138 before treatment start and three weeks into the treatment course. Visualised delineated volumes on the scans are the critical structures, parotid glands and spinal cord, as well as the body outline. On the scan obtained before treatment start, the matching volumes are shown. At ReCT the delineated volumes from pCT and ReCT are shown together. The bold volumes match the ReCT.

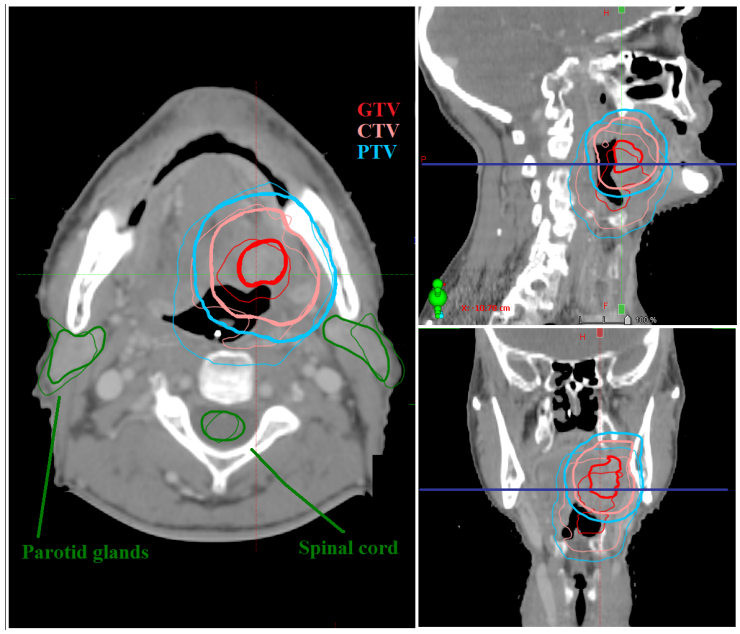

Figure 2.11: ReCT. The visualised delineated structures are the organs at risk, parotid glands and spinal cord, as well as the target structures. Delineated volumes from pCT and ReCT, shown together. The bold volumes matches the ReCT. Patient ID 134

Chapter 3

Previous work

Following chapter introduce previous work related to this study. DIR used for adaptive radiation therapy are topic for much related work, however two specific studies are chosen as main subject for this chapter. The first study mentioned serves as inspiration for the method and measures employed in this thesis. The second study performs DIR between CBCT and CT and served as a foundation for the additional work performed in this thesis.

3.1 Dosimetric evaluation of automatic segmentation for adaptive IMRT for head-and-neck cancer by Tsuji et al.

The work performed by Tsuji et al. [44] on his paper from 2010 compares, automatic and manual delineation of structures and DVH points from adaptive treatment plans. The study was performed on 16 patients with H&N cancer treated with IMRT.
Structures were delineated manually by a physician, and acquired automatically by using commercially available software. The software deformed the structures of the initial planning CT to a midterm CT, and was based on an intensity-based-free-form DIR algorithm. The deformed structures made base for an

auto adapted plan using the same planning constrains as in the original plan. [44].
The delineated structures were compared using Dice similarity coefficient (DCS) and an overlap index (OI). Dosimetric comparison was based on different DVH points and a conformal index.
The procedure of DIR used in the study by Tsuji et al. is comparable to the one used in this study. However in this study registration is based on CBCT and CT, where Tsuji et al performed CT-to-CT registration.
Where Tsuji et al. used DSC, OI and volume of the structure for evaluation; the center of mass shift (COM) is also included in our study.
The dosimetric evaluation performed by Tsuji et al. is based on a reoptimized plan used on the deformed image, however still using the same planning contains. The difference between manual and auto plans therefore primarily originates from the optimization and the structures. In this study, the initial plan is transferred to ReCT and dCT without any optimization to make the effect of different structures more comparable.

Tsuji et al.[44] finds that that automatic contours are not robust enough to replace manual contours, especially with respect to GTV and CTV. Additionally is found that automatic contours for OAR can be used without compromising the plan quality [44].

3.2 Deformable planning CT to cone-beam CT image registration in head-and-neck cancer by Hou et al.

Hou et al.[29] used automatic delineation of structures based on DIR in his study from 2011. The DIR used was based on the symmetric forces demons algorithm. The study was performed on 12 patients with H&N cancer. The image registration was performed between CT and CBCT. Prior to the DIR, a normalization of the voxel intensity was performed using histogram matching. This was performed due to CBCT and CT having difference in intensities. The registration was evaluated by using target registration error (TRE) and DSC[1].
Nine anatomical points where chosen by an experienced oncologist and annotated on the CT and the CBCT. TRE was determined by deriving the difference between the deformed points and the original points. DSC was determined between GTV of the CT and the deformed image [29].
The same procedure for DIR is used in present study, however without the normalization of intensities in the images. The normalization is not performed,

[1] By Hou et al. called volume overlap index (VOI)

due to no such requirement of pre-processing by the software used. Hou et al. evaluates the geometrical differences between the initial CT and the deformable CT. Our study will in addition to this also compare dosimetric difference.

Hou et al. [29] found the accuracy of the image registration to be near a voxel size and concluded that DIR have the potential to be used as an automatic tool for structure delineation.

Chapter 4

Materials and methods

4.1 Data

This retrospective study includes data from seven H&N cancer patients. The data consist of a planning CT (pCT), a CBCT from the middle of the treatment course, and a new CT (ReCT) acquired approximately at the same time as the CBCT. The two CT data sets both includes a structure set, containing the manually delineated structures. pCT also have an approved IMRT plan available conducted in the TPS, Eclipse (Varian Medical Systems, v.10.0). The calculation of dose is based on the *Anisotropic Analytical Algorithm* (AAA). All treatments have been performed on a Varian, Clinac iX, linear accelerator. Data originates from patients believed to have experienced anatomical changes during their treatment courses.
Table 4.1 shows an overview of patients included in this study. The table contains information about the *primary site* of the tumour which for five of the patient is placed in the oropharynx, the middle part of the throat. Patient 131 have a tumour marked as occult, meaning the origin of the tumour is unknown. Patient 134 have a tumour marked as OrisPrim, meaning that tumour is placed in the oris cavum (oral cavity) and no surgical removal of the tumour have been performed (prim). *Site* represents the placement of the tumour, sinister(sin) or dexter(dxt). *Dose* is the prescribed dose, which for six of seven patients is 68Gy. Each prescribed dose is divided into *fractions*, meaning the patient receives 2

Gy pr. fraction, and this will result in 34 fractions (times of treatment) for a patient with a prescribed dose of 68Gy. Each patient received six fractions a week.
The fraction at which the CBCT and ReCT were conducted is available in the last two columns (Table 4.1). For two patients, the CBCT and ReCT were not conducted at the same day but with one day between them. It is assumed that no significant changes have occurred between the two fractions. The procedure is to conduct a CBCT at midterm treatment. This means CBCT and ReCT should be obtained around fraction number 17, which is the case in four of the patients. Three patients received their scans later in the treatment course, at a near-end treatment point. Since this study will not focus on when replanning should be conducted, these scans from later fractions can be used on equal terms with the ones conducted around fraction number 17.

Table 4.1: Overview of patients used in this study

Patient Id	Gender/Age	Primary site	Site	Dose [Gy]	Fractions	CBCT [Frac]	ReCT [Frac]
131	M/76	Ocult	Sin	68	34	17	18
133	F/56	Oropharynx	Dxt	68	34	17	17
134	M/63	OrisPri	Sin	68	34	17	17
135	F/56	Oropharynx	Dxt	68	34	18	18
136	M/57	Oropharynx	Sin	66	33	29	29
137	F/75	Oropharynx	Sin	68	34	24	24
138	M/67	Oropharynx	Dxt	68	34	23	22

4.2 Data Processing

The data is anonymized using the ConQuest DICOM server version 1.4.16 [7]. When the data is anonymized, and cleared of any personalized information it is further processed in *SmartAdapt*® (v. 11.0) on a computer in a *"stand alone"* system. The stand-alone system is called a training box (T-box). The T-box also have the TPS *Eclipse*® (v.10.0) available. *SmartAdapt*® is used for image registration whereas *Eclipse*® is used for calculation of the dose distribution.

This study consists of three parts:

A: DIR based on ReCT and CBCT - Performed to examine the algorithms dependency on the modality used for registration.

B: Geometric and dosimetric comparison of DIR based CBCT (dCT_{CBCT}) and ReCT - Performed to evaluate structures generated by the DIR compared to manually delineated structures, as well as to determine if the deformable image and structures are suitable for dose calculation.

C: CBCT-based dose calculation - Performed to evaluate dose calculation based on CBCT compared to CT.

The basis for this thesis is further outlined in Figure 4.1.
The geometric and dosimetric comparison of dCT_{CBCT} and ReCT will be the main focus of this thesis and the method used, is based on this comparison (Figure 4.1B).

4.2.1 Image Registration - Performed in *SmartAdapt*®

In order to make the DIR between images in *SmartAdapt*®, an initial rigid registration is required by the software.

Rigid image registration

The pCT scan is marked as the source image and the CBCT is set as the target image prior to the registration. First part of the registration is performed manually by the user, who moves the CT to match the CBCT. The manual registration is performed mainly by bone-alignment.

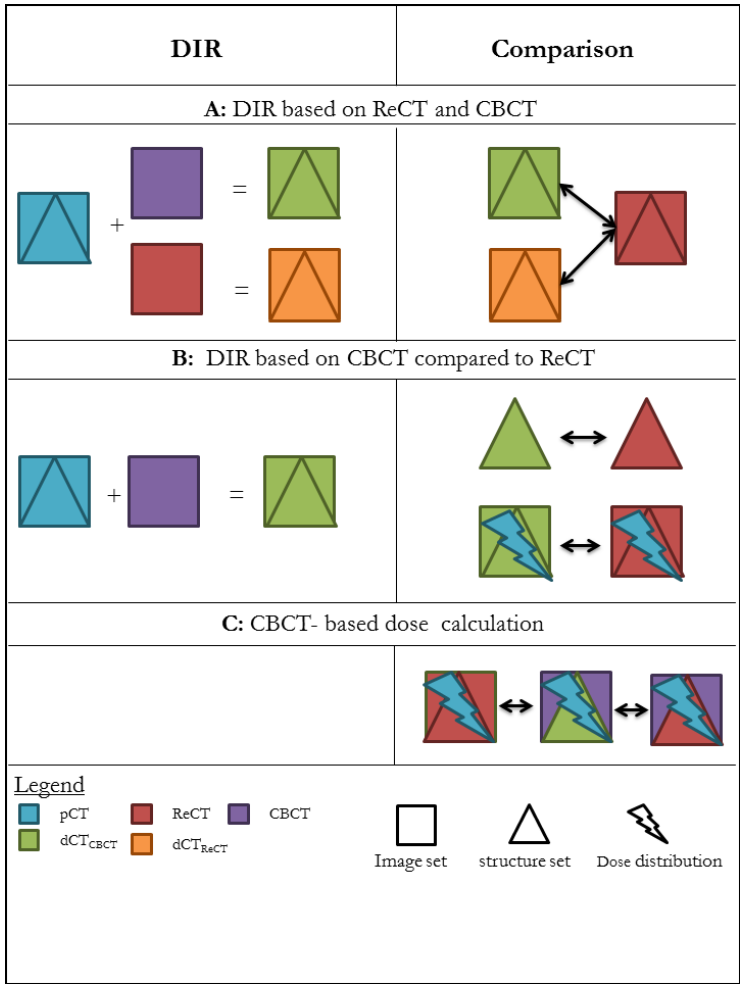

Figure 4.1: Overview of studies performed in this thesis. Illustrates the how the DIR has been performed in each study and what the comparison is based on. Arrows pointing in both directions, symbolises a comparison. Each image type has been divided into colours, and images, structure set, and dose distribution has each been assigned a simple figure

An automatic rigid registration is used to refine the registration. The registration is based on translation and rotation, however rotation will be ignored, due to limitations of the TPS, *Eclipse*®. Some rotation might occur in the images, but will be compensated by the DIR. The similarity measure, used for the rigid registration, is mutual information[1]. Figure 4.2 illustrates pCT and CBCT together after registration has been performed.

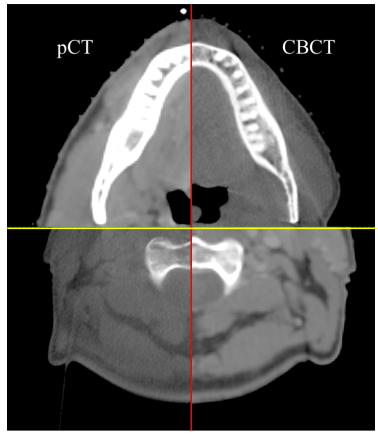

Figure 4.2: Split window, showing the registered pCT and CBCT. The outline do not match due to CBCT being conducted three weeks in the treatment period, and patient having experienced i.a tumour and weight loss. Patient ID: 136

Deformable image registration

Following initial rigid image registration is the deformable registration procedure. Deformable registration is based on the Demons algorithm as described in Section 2.4 [47]. The registration performed within a defined volume of interest (VOI), is chosen to match the dimensions of the smallest of the two image sets. The image acquisition of the CBCT leads to a scan range smaller than the one for CT, and the dimensions of the CBCT will be the decisive factor for the VOI. The image registration produces a new image set containing the image quality of the CT and the structural information of the CBCT.

[1] Chosen in the *SmartAdapt*® options

When the DIR is performed the structures from the pCT is propagated to the registered image set. The propagation will deform the structures by applying the deformation field to the original structures. The result will be a deformed image set with corresponding structures. The structures on the dCT_{CBCT}, is visually inspected to ensure the registration has been done correct. In some cases small abnormalities are observed. This will typically be extra tissue due to a bolus[2] on the patient during treatment or the thermoplastic mask. This will 'trick' the algorithm to believe the patient has more tissue in the local area. *SmartAdapt*® provides a tool called *deformation field correction* that makes it possible to manually correct in places where it is assumed that the deformation is incorrect.

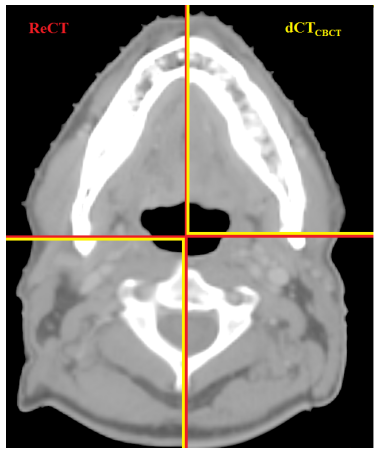

Figure 4.3: Split window, showing the registered dCT_{CBCT} and ReCT. Illustrates the quality of the deformed image compared to ordinary CT image

Once the deformation is accepted, the image set will be exported from *SmartAdapt*®. The exportation is performed in order to obtain a new image set.
The new image set of dCT_{CBCT} is reimported to *SmartAdapt*®, and a manual followed by an automatic rigid registration will be performed between the dCT_{CBCT} and the ReCT.
Figure 4.3 illustrates dCT_{CBCT} together with ReCT in a split window. The dCT_{CBCT} is visually very similar to ReCT.

[2] A bolus consist of a tissue equivalent material and is placed directly on the skin of the patient to provide a flat surface of the beam. A bolus is used to account for the effect of the depth-dosis [39]

4.2.2 Dose Calculation - Performed in *Eclipse*®

The clinically treatment plan, based on pCT is used for dose calculation on ReCT and dCT_{CBCT}. This is done to compare the dCT_{CBCT}-based dose plan with the one based on ReCT. The treatment plan is transferred to ReCT and dCT_{CBCT} and calculation of dose is performed. The dose calculation is performed with present values by the use of fixed monitor units (MU).

4.2.3 Deformable image registration based on ReCT and CBCT

A rigid registration as well as DIR is performed as described above. For this substudy the image registration is performed between pCT - ReCT and pCT - CBCT (Figure 4.1A). Structures of ReCT were removed prior to the image registration. A new deformed structure set, is applied to dCT_{ReCT} and dCT_{CBCT}, respectively. The deformed structure set is obtained by applying the deformation field, derived by the DIR, to the structures of pCT. Geometrical measures are determined between the deformed structures and the manually delineated structures of ReCT. The goal of this substudy is to evaluate if the DIR depend on the modality used.

4.2.4 CBCT-based dose calculation

In this substudy dose calculation is based on the CBCT image set with deformed structures from dCT_{CBCT}, and the manually delineated structures from ReCT (Figure 4.1C). Dose is calculated, using the same settings as for the pCT-based plan.

4.3 Evaluation tools

The main objective of this thesis is the comparison between dCT_{CBCT} and ReCT, based on geometric and dosimetric measures. The substudies described in Section 4.2.3 and 4.2.4 will be evaluated using the same measures.
The geometrical comparison will be based on simple volume assessment, COM, DSC and OI. The collection of measures should make it possible to determine if the structures made from the DIR are similar to the manually delineated ones.

Treatment plans are evaluated to ensure optimal tumour control and minimum dose to normal tissue and OAR. The dosimetric comparison will in this thesis be based on dose statistics from dose volume histograms-(DVH), and conformity index (CI), normal tissue overdosage fraction (NTOF) and lesion coverage fraction (LCF) [39].

4.3.1 Geometrical measures

The geometrical comparison is based on selected structures. Target structures are GTV, CTV and PTV, for tumour. The selected OAR are chosen based on existence of the structure on CBCT and delineation on pCT. Parotid glands and spinal cord were for all patient delineated and part of the CBCT, and therefore chosen for basis of geometrical comparison.

Simple volume assessment
The volume is chosen as a geometrical measure to present the difference between two volumes. This is chosen because it is easily understood and free from bias [25]. However simple volume assessment, lack the ability to evaluate the spatial location.

Center of mass shift
The spatial evaluation can be obtained by the use of COM, which can be used to describe the displacement between the locations of two structures. The center of mass shift is provided by *SmartAdapt*® as the displacement in the x, y, and z-direction. In order to collect these numbers the length of the displacement vector is determined by use of:

$$|COM| = \sqrt{x_{COM}^2 + y_{COM}^2 + z_{COM}^2} \tag{4.1}$$

COM has a drawback since it does not take the shape of the structure into account. This means that two very different shapes can obtain similar COM (Figure 4.4(b),(c)). Structures of same size and shape can obtain a falsely result

of COM. This will occur if the two structures are e.g. perpendicular to each other (Figure 4.4(a)). Therefore measures accounting for the union between two volumes are chosen as well. These two measures are DSC and OI.

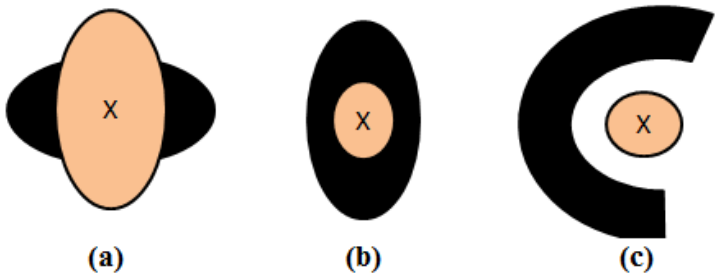

Figure 4.4: Centre of mass examples. *(a)* show two volumes of same size and shape, but different orientation. *(b)* Two volumes of different size and shape, but identical COM. *(c)* illustrates a target volume with a curved shape where the centre of mass is outside the volume. Inspired by [25]

Dice similarity coefficient
DSC is a simple measure for the volume included in both of the volumes of the delineated structure [19].
DSC is defined as:

$$\mathrm{DSC} = \frac{2(V_{ReCT} \cap V_{dCT(CBCT)})}{V_{ReCT} + V_{dCT(CBCT)}} \tag{4.2}$$

Where $\mathrm{V_{dCT(CBCT)}}$ is the volume of a structure in the deformed CT image and $\mathrm{V_{ReCT}}$ is the volume of the corresponding structure in ReCT. DSC represents the union of the two volumes divided by the average size of the two volumes. If the structures are overlapping 100%, the union of the two volumes will be of same size as the average of the two volumes. This will result in a value of one indicating full overlap. Zero will indicate no overlap [25]. DSC has the drawback of not accounting for how the structures are overlapping, this must be interpreted by visual evaluation of the structures. DSC is directly provided by *SmartAdapt*®.

Overlap Index
OI is defined as:

$$\mathrm{OI} = \frac{V_{ReCT} \cap V_{dCT(CBCT)}}{V_{ReCT}} \tag{4.3}$$

OI is used to complement the DSC, because DSC does not preference between ReCT and $\mathrm{dCT_{CBCT}}$. The ReCT is defined as the ground truth and by using

OI it is possible to determine the amount of V_{ReCT} within the $V_{dCT(CBCT)}$. It should be noticed that an ideal OI would falsely occur if V_{ReCT} was completely included in the volume of dCT_{CBCT}, as in Figure 4.4(b). This means that an ideal OI value can be obtained even though the structures are not identical. The volume of $V_{ReCT} \cap V_{dCT(CBCT)}$ is found by using the Boolean operator function available in *SmartAdapt*®.

4.3.2 Dosimetric measures

DVH
When composing a treatment plan, the dose information provided in a 3D matrix will reflect dose in a defined volume. As this can be difficult to evaluate, the DVH is used to easily summarize the dose information [39].
DVH represents the defined volume receiving a specific dose, against a set of dose intervals, resulting in a graph with volume on the ordinate and dose on the abscissa. Values of volume and dose can be presented as relative and/or absolute [39].
DVH can be presented as differential or cumulative, where the cumulative is the most frequently used. The differential DVH shows the relative or absolute volume in the dose intervals, like in a regular histogram. The cumulative DVH shows the volume receiving a dose greater than or equal to a given dose. The first bin will contain 100% of the volume because the full volume always receives at least zero dose. The last bin contains the volume receiving the maximum dose. The optimal distribution for target and OAR is illustrated in Figure 4.5B, illustrating that 100% of the target volume optimally receives maximum dose, and 100% of the OAR receives zero dose. Practically this is not possible because of the positioning of the tumour, which will often be very near the OAR (Figure 4.5A), [36, p. 722-724],[31].
DVH is used as an evaluation tool, to compare different dose plans for selected targets and OAR. However, when comparing plans, care should be taken, as DVH only provides information about the dose distribution within a structure, and do not include spatial information. This means that the DVH does not reflect if there are several areas with high or low dose or just one large one. Interpretation of a DVH is rather subjective and small differences between DVHs are hard to quantify. To overcome this problem biological models, such as tumour control probability (TCP) and normal tissue complication probability (NTCP), can be used to rank the plans [36, p. 727]. However, this is beyond the scope of this study.

Dose statistics To quantify the results from the DVH different points in the graph are chosen to represent the dose distribution within the target or OAR,

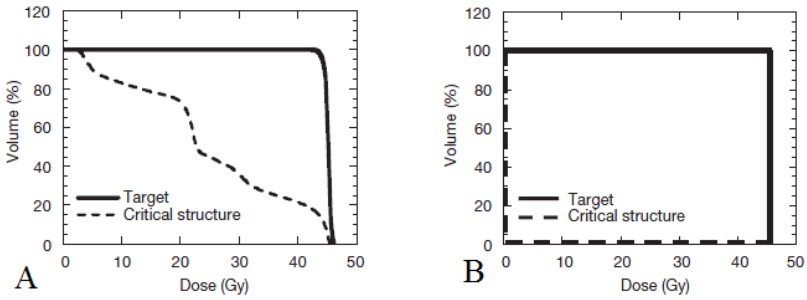

Figure 4.5: Cumulative DVH. *A:* Example of realistic DVHs for target and critical structure. 100% of the target volume receives maximum dose *B:* Ideal DVHs for target and critical structure. For the target 100% of the volume is receiving maximum prescribed dose, and the critical structure is receiving zero dose for 100% of the volume [39]

these are called DVH-points. By evaluating the DVH-points, it is possible to determine if the target structure receives the prescribed dose and the OAR receives a dose that is below the defined tolerance level [36]. DVH-points are a simplified view of the delivered dose, and make it easy to compare different plans. Journal of the ICRU Report 83 have suggested some specific dose constrains for the target structures[3][31, 17] and following are used for evaluation in this study:

- $D_{2\ \%}$: Maximum absorbed dose covering 2% of the volume
- $D_{95\ \%}$: Minimum absorbed dose covering 95% of the volume
- $D_{50\ \%}$: Absorbed dose received by 50% of the volume

For OAR:

- D_{mean} : Mean absorbed dose in the structure
- D_{max} : Maximum absorbed dose to the structure

Depending on the type of OAR different measures should be used. The OAR can be divided into parallel-like or serial-like organs, which is an analogy to an

[3]Target will in this study, where nothing else is mentioned, be defined as GTV-T, CTV-T and PTV-T

electrical circuit (Figure 4.6). Parallel-like organs have sufficient capacity to overcome larger damage [31]. In analogy with the electrical circuit, the circuit (organ) still function, if one resistor breaks (damaged organ tissue). A mean absorbed dose D_{mean} is used as dose constrains for parallel like organs.
Serial-like organs do not have the capacity to handle damage. The dose should therefore always be below a specific tolerance level and the maximum dose should be evaluated. The DVH is provided by the TPS and DVH points are found by evaluating the histogram.

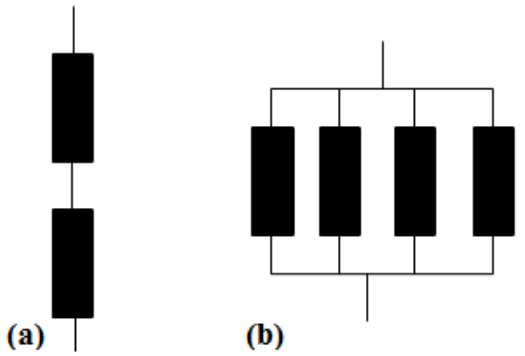

Figure 4.6: OAR tolerance in analogy with an electrical circuit. *(a)* Resistors connected in series. If one single resistor is defect the entire circuit will be broken and no current can flow. Spinal cord, a serial organ, will lose the function if only a small part gets damage (b) Resistors connected in parallel. The circuit will still work if one resistor breaks, however not as well. Parotid glands, a parallel organ, will maintain some function, even though some of the tissue is damaged. Inspired from [31]

Conformity index

CI is a measurement for plan conformity developed by the Radiation Therapy Oncology Group (RTOG)[24]. When evaluating the plan, CI can be used to give an assessment of the dose coverage of the target structure and healthy tissue. The CI uses geometric features to describe the amount of overlapping between two irradiated volumes [24]. The CI is a measure for how well the target volume is covered by an isodose line. Isodose curves are lines presenting the dose distribution. A specific isodose line can be converted into a structure by the TPS. This will make it possible to determine the size of the volume of tissue, receiving a specific dose. This value can also be found on the DVH.

CI is defined by:

$$\mathrm{CI} = \frac{V_{95}}{V_{PTV}} \tag{4.4}$$

Where $\mathrm{V_{95}}$ is the volume covered by the 95% isodose, and $\mathrm{V_{PTV}}$ is the PTV volume. Ideally, no irradiation should exceed this volume.
This index will typically range from 0-2. In case of perfect conformation, CI equals one. A CI greater than one is obtained when the treated volume is larger than the target volume. A CI below one is obtained when the target is only partly covered [24].
CI has the drawback of not taking the spatial intersection of the volume or the shape into account. This means that CI can obtain a value of 1, without any overlap between the two volumes (Figure 4.7A). Therefore, it is important to visually confirm that the structures are overlapping. Additional measures will in this study be used to assist CI. The measures chosen are LCF and NTOF [46].

Lesion coverage fraction
LCF is an expression for the fraction of the PTV covered by the 95% isodose line. To find the fraction of PTV covered by the isodose a Boolean operator available in the TPS, is used to make a structure called *"PTVand95"*. This structure will include all pixels belonging to the PTV structure and the 95% isodose structure. In cases where the patient has two or more defined PTV's, these are included into *"PTV total"*. LCF is defined as:

$$\mathrm{LCF} = \frac{V_{PTVand95}}{V_{PTV}} \tag{4.5}$$

If the PTV is completely included in the 95% isodose, the LCF will equal unity [46].

Normal tissue overdosage fraction
NTOF is an expression for the fraction of the 95% isodose delivered to normal tissue and is defined as:

$$NTOF_{95} = \frac{V_{PTVsub95}}{V_{95}} \tag{4.6}$$

Where $\mathrm{V_{95subPTV}}$ is the volume of the 95% isodose structure subtracted all pixels included in the PTV. If the 95% isodose encircle the PTV perfectly, the target will receive the prescribed dose, and no normal tissue will receive high dose irradiation. This will result in a NTOF of zero [46]. NTOF will also obtain the value of zero if the 95 % isodose is inside the PTV. This gives the ideal value of NTOF, but the target is not sufficiently covered, see figure 4.7B. Therefore NTOF should be compared to the LCF to ensure acceptable values for both measures.

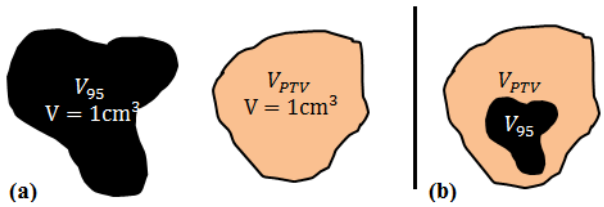

Figure 4.7: *A:* Illustration of the drawback of CI. No spatial correlation is found between the two structures, but the illustrated case would result in an ideal value of CI. *B:* Illustration of the drawback of NTOF. If the 95%isodose is inside the PTV, NTOF will obtain the ideal value. This results in insufficient coverage of the target structure which is undesirable.

4.3.3 Statistical analysis

Statistical analysis has been performed for some of the measures to investigate the significance of the findings. All statistical analysis has been performed in the statistical software *"R"* Version 2.12.2 [8]. Prior to any statistical analysis, data is investigated in order to determine if it is normally distributed. This is done by visual evaluation of quantile-quantile plots (QQ-plot) provided by the software, as well as a Shapiro-Wilks normality test. The null-hypothesis of the test, is data being normally distributed at a significant level of α=0.05 [41]. If data are normally distributed data points in the QQ-plot will be linear related (Figure 4.8).

Data found to be normally distributed and equal in variance will be compared by a paired t-test or an analysis of variance (ANOVA).
The paired t-test is used to test for difference in mean values, of two related groups. The level of significance is chosen to be $\alpha \leq 0.05$
The ANOVA is used when the mean of more than three groups are compared [37].
When data is found to not be normally distributed a Wilcoxon rank sum test will be used. This test is the non-parametric alternative to the paired t-test[37].
The chosen test for analysis will be included in the results tables in the following chapter.

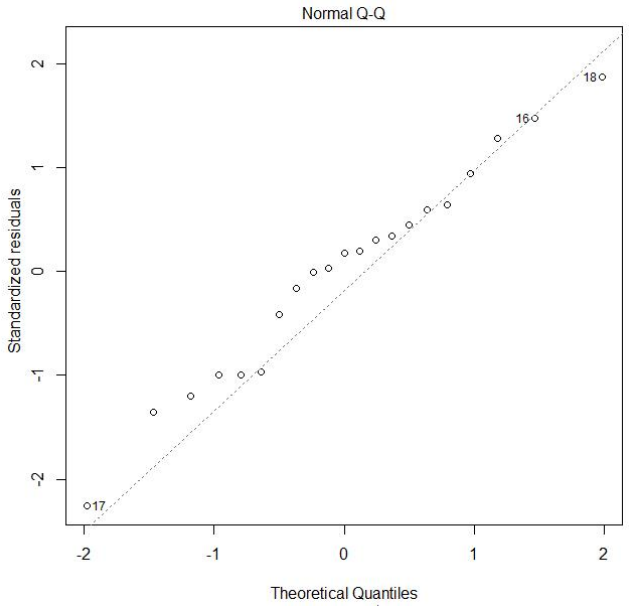

Figure 4.8: QQ-plot for PTV D_{95}

Chapter 5

Results

In this chapter results from the data analysis will be presented. Data originates from seven patients with H&N cancer as explained in Chapter 4.1. This chapter is divided into three major sections:

A: Geometrical evaluation of DIR based on CBCT and ReCT

B: Geometrical and dosimetric comparison of d_{CBCT} and ReCT

C: CBCT-based dose calculation

5.1 Deformable image registration based on ReCT and CBCT

This section presents the results of DIR based on CBCT and ReCT respectively. The DIR is performed between pCT-ReCT and pCT-CBCT, each without any delineated structures. This is done to examine whether the registration is dependent on the image modality used. In the following dCT_{CBCT} and dCT_{ReCT} will be compared to ReCT with manually delineated structures (Figure 4.1A). To investigate if the DIR is independent on the modality used, the desire is to

obtain similar results for dCT_{CBCT} and dCT_{ReCT}.

Similar results between dCT_{CBCT} and dCT_{ReCT} are observed for GTV with regard to values of COM, volume difference and DSC (Figure 5.1).

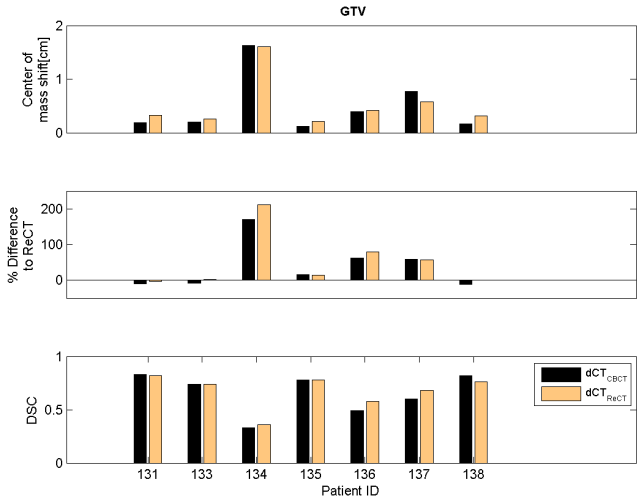

Figure 5.1: GTV. Geometrical comparison between dCT_{CBCT} and dCT_{ReCT} relative to ReCT. *Top:* COM with respect to ReCT *Middle:* Percentage-wise deviation in volume with respect to ReCT. *Bottom:* DSC for dCT_{CBCT} and dCT_{ReCT} with respect to ReCT

The difference in estimated volume is for patient 135 and 137 found below 2%. By taking all patients into account a difference below 13.5% is observed. Similar tendency is observed for CTV and PTV, see Appendix C. GTV represent the tumour volume and is chosen as the visualised structure because, CTV and PTV ideally should be derived from the size and shape of GTV.

The parotid glands show some difference between dCT_{CBCT} and dCT_{ReCT} with regard to values of COM and volume difference (Figure 5.2(a) and 5.2(b)). Values of DSC is relatively close for both parotid glands. The result of a paired t-test, for COM and DSC, show no significant difference in mean between dCT_{CBCT} and dCT_{ReCT} (Table 5.2). It should however be noticed that the standard deviation for COM is larger than for DSC.
For all three measures no similarity between the values of dCT_{CBCT} and dCT_{ReCT} is found for the spinal cord (Figure 5.3). The paired t-test supports this, since the p-value for DSC is significant (Table 5.2). However no

Table 5.1: Volume of GTV and percentage-wise difference to dCT_{ReCT}

Patient ID	*Volume [cm^3]*		
	dCT_{CBCT}	dCT_{ReCT}	difference%
131	97.0	105.3	-7.9
133	3.2	3.7	-13.5
134	15.7	18.1	-13.3
135	5.9	5.8	1.7
136	4.7	5.2	-10.6
137	29.2	28.8	1.4
138	12.2	13.9	-12.2

Table 5.2: Geometrical measures for OAR, Test = paired t-test, $\alpha \leq 0.05$

	Parotid dxt		*p-value*
	dCT_{CBCT}	dCT_{ReCT}	
COM	0.42±0.17	0.34±0.10	0.30
DSC	0.74±0.05	0.77±0.08	0.28

	Parotid sin		*p-value*
	dCT_{CBCT}	dCT_{ReCT}	
COM	0.41±0.22	0.38±0.12	0.64
DSC	0.73±0.09	0.76±0.07	0.12

	Spinal cord		*p-value*
	dCT_{CBCT}	dCT_{ReCT}	
COM	1.05±0.73	0.56±0.45	0.05
DSC	0.67±0.10	0.79±0.04	0.01

statistical difference for mean values of COM are observed. Again it should be noticed that the standard deviation is quite high. The value of DSC is for every patient estimated larger for $\mathrm{dCT}_{\mathrm{ReCT}}$ than $\mathrm{dCT}_{\mathrm{CBCT}}$.

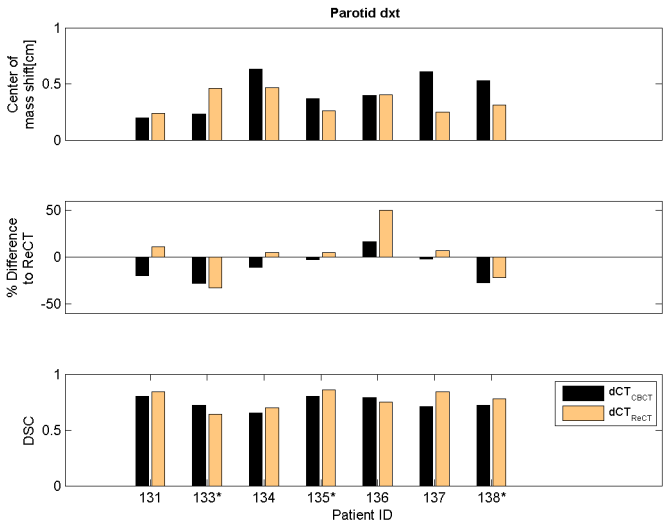

(a) Geometrical measures for Parotid dxt. Patient with primary tumour site dex is denoted with a *

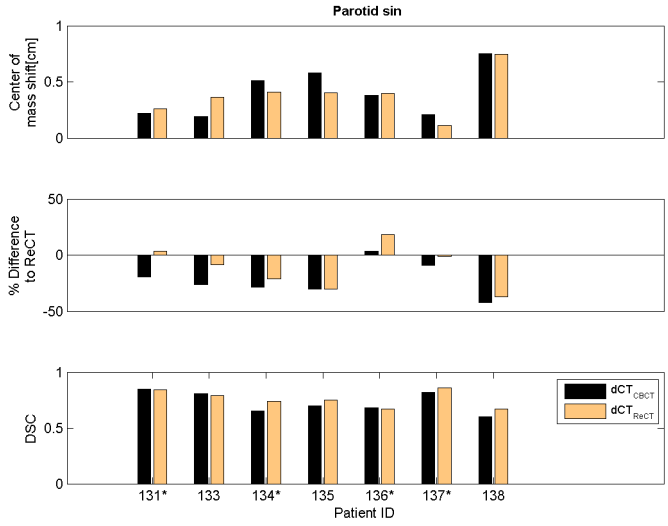

(b) Geometrical measures for Parotid sin. Patient with primary tumour site sin is denoted with a *

Figure 5.2: Geometrical comparison between $\mathrm{dCT}_{\mathrm{CBCT}}$ and $\mathrm{dCT}_{\mathrm{ReCT}}$ relative to ReCT. *Top:* COM for $\mathrm{dCT}_{\mathrm{CBCT}}$ and $\mathrm{dCT}_{\mathrm{ReCT}}$ with respect to ReCT. *Middle:* Percentage wise deviation in volume with respect to ReCT. *Bottom:* DSC for $\mathrm{dCT}_{\mathrm{CBCT}}$ and $\mathrm{dCT}_{\mathrm{ReCT}}$ with respect to ReCT

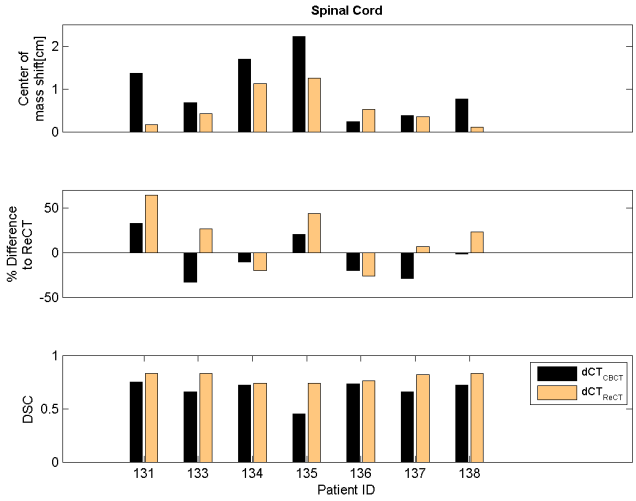

Figure 5.3: Spinal Cord. Geometrical comparison between $\mathrm{dCT}_{\mathrm{CBCT}}$ and $\mathrm{dCT}_{\mathrm{ReCT}}$ relative to ReCT. *Top:* COM for $\mathrm{dCT}_{\mathrm{CBCT}}$ and $\mathrm{dCT}_{\mathrm{ReCT}}$ with respect to ReCT *Middle:* Percentage wise deviation in volume with respect to ReCT. *Bottom:* DSC for $\mathrm{dCT}_{\mathrm{CBCT}}$ and $\mathrm{dCT}_{\mathrm{ReCT}}$ with respect to ReCT

5.2 Comparison of dCT_{CBCT} and ReCT

This section presents the results of DIR based on CBCT, compared to ReCT with manually delineated structures. The comparison is performed to determine if the DIR performs similar to the physician. The comparison is divided into geometric and dosimetric measures (Figure 4.1B).

5.2.1 Geometrical comparison

The values of COM is found to be below 1cm for six of seven patients for the GTV (Figure 5.4). Patient number 134 shows a large displacement and obtains a very low value of DSC. The volume of GTV estimated by the physician is $32.6cm^3$ smaller than the DIR found using dCT_{CBCT} (Table 5.3). This results in the large percentage-wise deviation in volume from ReCT observed in Figure 5.4. Figure 5.6 illustrates the structures from the DIR and those conducted by

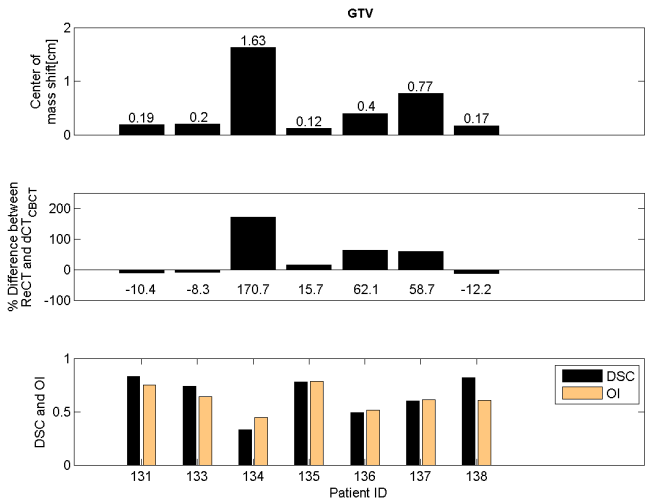

Figure 5.4: Geometrical measures for GTV. *Top*: Center of mass shift between ReCT and dCT_{CBCT}. *Middle*: Percentage wise deviation in volume of dCT_{CBCT} with respect to ReCT. *Bottom*: DSC and OI determined between dCT_{CBCT} and ReCT

the physician. It is found that the physician has estimated a large and asymmetrical shrinkage of the tumour. This gives rise to the large difference between

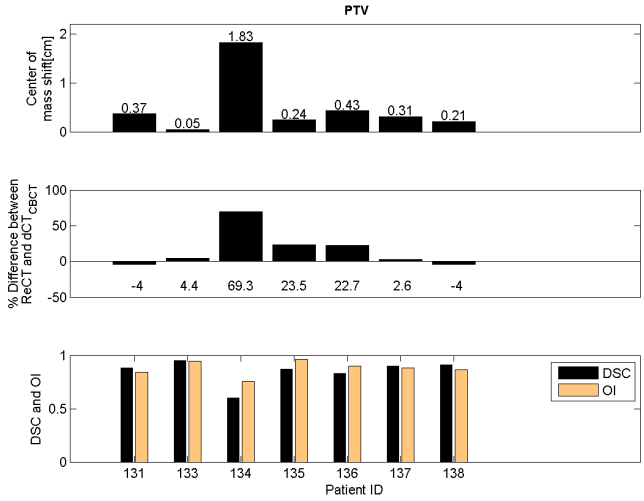

Figure 5.5: Geometrical measures for PTV. *Top*: Center of mass shift between ReCT and $\mathrm{dCT}_{\mathrm{CBCT}}$. *Middle*: Percentage wise deviation in volume of $\mathrm{dCT}_{\mathrm{CBCT}}$ with respect to ReCT. *Bottom*: DSC and OI determined between $\mathrm{dCT}_{\mathrm{CBCT}}$ and ReCT

dCT_{CBCT} and ReCT, for GTV, CTV and PTV. The low value of DSC, and large COM for patient 134 in previous section (5.1) is also caused by this. The manually delineated structures on pCT and ReCT was subsequently confirmed by a physician, and found to be correct in both scans. The large difference arises from the placement of the tumour (oral cavity). As the tumour became smaller, more mobility was obtained by the tongue, hence the asymmetrical shrinkage [1]. No trend was found for values of DSC or OI, with respect to the GTV.

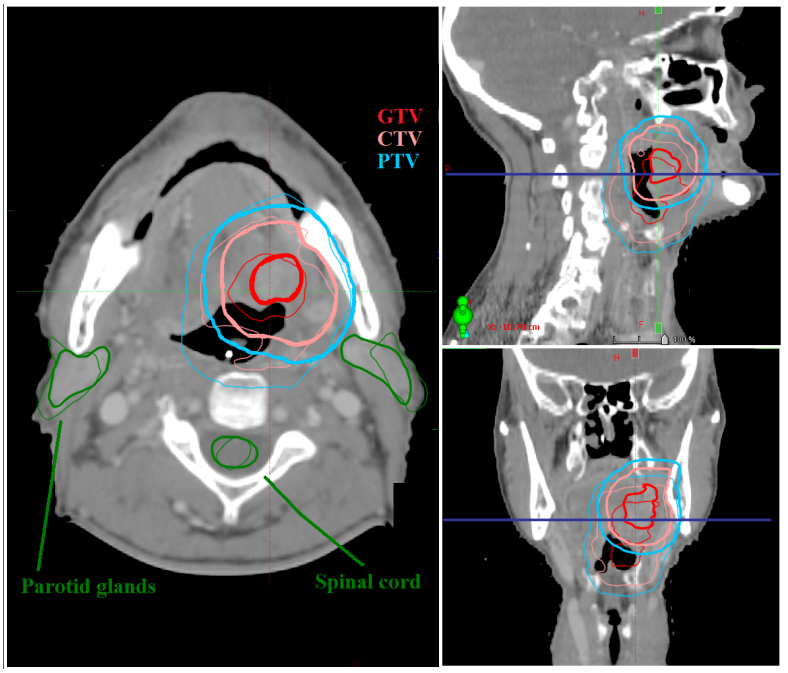

Figure 5.6: ReCT. Deformed structures is shown together with manually delineated structures, to visualise the difference. Manually delineated structures are marked with a bold line. Patient ID:134

For all patients, except the outlier, patient 134, it is found that the values of COM for PTV is below 0.5cm. DSC and OI obtains high values indicating a large similarity of dCT_{CBCT} and ReCT (Figure 5.5). The percentage-wise difference in volume from ReCT are below 5% for patient 131, 133, 137 and 138. The negative percentage wise difference from ReCT, observed for patient 131 and 138 reveals that ReCT has estimated the volume higher than dCT_{CBCT}. The estimated volumes are found to be close for nearly all patients. However the PTV is estimated larger for dCT than ReCT for five of the seven patients. The volume is estimated larger than the initial scan by the DIR for patient 133

[1] Oral conversation with physician Christian Maare

and 135 (Table 5.4).
Results for CTV is similar to those for PTV, however with a tendency of a bit lower values of DSC (range, 0.54-0.89) and OI (range, 0.66-0.90). See Appendix C.

Table 5.3: Volume of GTV

Patient ID	*Volume* $[cm^3]$		
	pCT	dCT_{CBCT}	ReCT
131	159.9	97.0	108.3
133	3.8	3.3	3.6
134	18.1	15.7	5.8
135	5.4	5.9	5.1
136	6.3	4.7	2.9
137	31.8	29.2	18.4
138	14.2	12.2	13.9

Table 5.4: Volume of PTV

Patient ID	*Volume* $[cm^3]$		
	pCT	dCT_{CBCT}	ReCT
131	608.9	502.8	523.8
133	128.0	132.9	127.3
134	163.6	159.5	94.2
135	90.1	99.2	80.3
136	85.6	80.0	65.2
137	241.8	231.2	225.3
138	139.9	133.2	138.8

Values of COM for parotid dxt is found to be large with values up to 0.63 cm (Figure 5.7). Percentage-wise volume difference to ReCT is below 17% for four out of seven patients (134, 135, 136, 137). For all patients expect 136 the volume is smaller for dCT_{CBCT} than for ReCT and pCT. DSC values are found to range between 0.65 and 0.80. Similar tendency are observed for parotid sin. OI obtains values between 0.57-0.77 for parotid dxt and 0.48-0.70 for parotid sin.
The volume of manually delineated parotid dxt, is estimated larger than pCT in patient 133 and 138 (Table 5.5). This means that the physician have expected the parotid gland to have grown. The same is observed for parotid sin in patient 134, 135 and 138.

A large spread in the size of COM for the spinal cord is observed with values ranging from 0.23cm to 2.2cm (Figure 5.9). Low values of DSC and OI is observed for all patients indicating a poor overlap between the structures. Percentage-wise volume difference to ReCT is found to obtain values up to 33%.

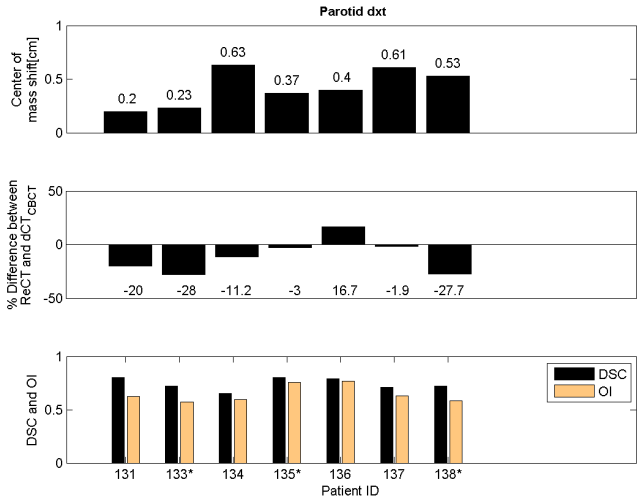

Figure 5.7: Geometrical measures for Parotid dxt. *Top*: Center of mass shift between ReCT and dCT_{CBCT}. *Middle*: Percentage wise deviation in volume of dCT_{CBCT} with respect to ReCT. *Bottom*: DSC and OI determined between dCT_{CBCT} and ReCT. Patient with primary tumour site dex is denoted with a*

Table 5.5: Volume of Parotid glands $[cm^3]$

Patient ID	*Parotid dxt*			*Parotid sin*		
	pCT	dCT_{CBCT}	ReCT	pCT	dCT_{CBCT}	ReCT
131	35.2	27.6	34.5	40.0	31.9	39.70
133	8.4	7.4	10.0	13.7	10.0	13.00
134	26.1	19.0	21.4	22.2	16.8	23.60
135	29.4	22.9	23.6	23.3	19.6	28.20
136	26.7	16.1	13.8	23.8	15.4	14.90
137	37.3	26.1	26.6	34.2	22.6	24.80
138	32.1	25.1	34.7	23.8	19.5	33.70

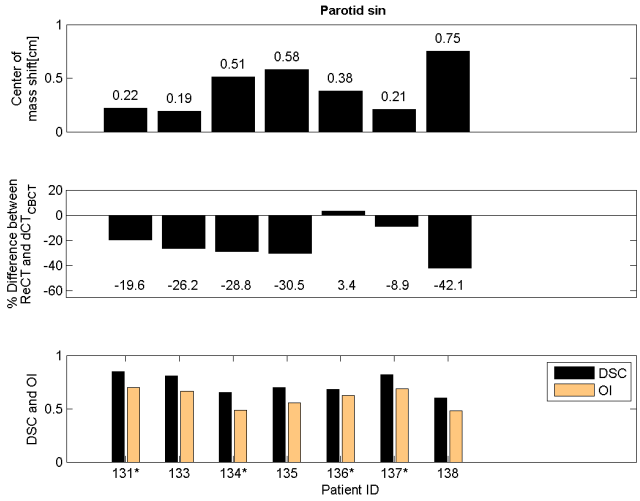

Figure 5.8: Parotid sin. *Top*: Center of mass shift between ReCT and $\mathrm{dCT}_{\mathrm{CBCT}}$. *Middle*: Percentage wise deviation in volume of $\mathrm{dCT}_{\mathrm{CBCT}}$ with respect to ReCT. *Bottom*: DSC and OI determined between $\mathrm{dCT}_{\mathrm{CBCT}}$ and ReCT. Patient with primary tumour site sin is denoted with a*

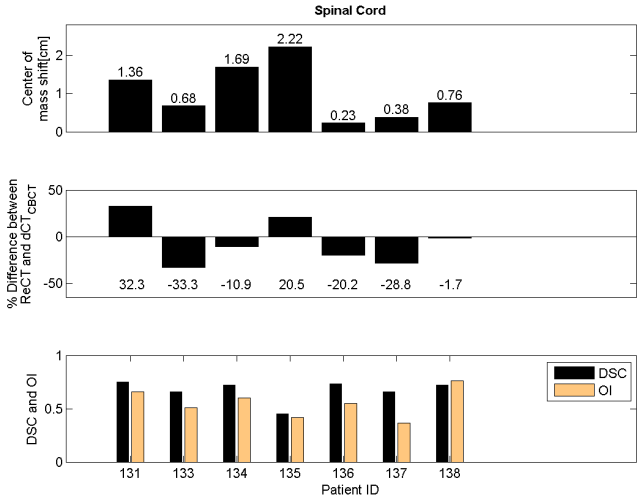

Figure 5.9: Geometrical measures for Spinal Cord. *Top*: Center of mass shift between ReCT and dCT_{CBCT}. *Middle*: Percentage wise deviation in volume of dCT_{CBCT} with respect to ReCT. *Bottom*: DSC and OI determined between dCT_{CBCT} and ReCT

Table 5.6 shows the average values of DSC and OI obtained in this study, and the one by Tsuji et al. [44].

Table 5.6: DSC and OI (mean±SD)

Structure	*DSC*		*OI*	
	-	Tsuji et al[44]	-	Tsuji et al[44]
GTV	0.66±0.19	0.69±0.12	0.62±0.11	0.6±0.17
CTV	0.81±0.13	0.78±0.10	0.83±0.07	0.77±0.08
PTV	0.85±0.12	-	0.88±0.66	-
Parotid dxt	0.74±0.05	0.72±0.09	0.65±0.08	0.71±0.08
Parotid sin	0.73±0.09	0.71±0.10	0.60±0.09	0.73±0.09
Spinal Cord	0.67±0.10	-	0.55±0.13	-

In order to compare the volume of dCT_{CBCT} and ReCT the volumes relative to pCT are determined (Table 5.7). Difference in mean between dCT_{CBCT} and ReCT are found not significant with respect to the target structures. With regard to the OAR does dCT_{CBCT} obtain a lower mean value than ReCT. Significant difference is only observed for parotid sin.

Table 5.7: Volume relative to pCT, test = paired t-test, $\alpha \leq 0.05$

	Mean relative volume±SD		
	ReCT	dCT_{CBCT}	p-value
GTV	0.70±0.24	0.85±0.14	0.16
CTV	0.83±0.17	0.9±0.11	0.174
PTV	0.86±0.14	0.97±0.08	0.116
Parotid dxt	0.87±0.21	0.75±0.07	0.08
Parotid sin	1.0±0.25	0.75±0.25	0.02
Spinal Cord	0.93±0.10	0.8±0.12	0.38

5.2.2 Dosimetric comparison

5.2.2.1 DVH points

The initial plan from pCT was transferred to ReCT and dCT_{CBCT}. The dose was calculated using fixed MU (Section 4.2.2). Figure 5.10 illustrates an example of a DVH for CTV. Difference between the DVH's of pCT, dCT_{CBCT} and ReCT is observed. From a DVH like this three points have been found for the PTV and CTV, D_{50},D_{95} and D_2, as seen in Table 5.8.

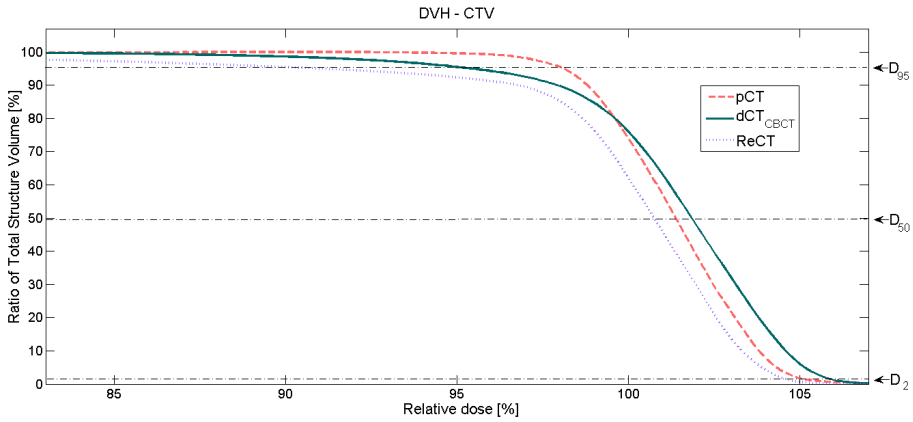

Figure 5.10: DVH for CTV, Patient ID: 136

The desire when replanning is that, the target always receives the prescribed dose to ensure maximum tumour control. Values are found to be of the same size for all DVH-points accordingly to the structure. A paired t-test conducted between dCT_{CBCT} and ReCT support this finding, since none of the DVH points are significantly different with a significance level (α) of 0.05, meaning that no difference in mean between dCT_{CBCT} and ReCT can be detected.

Table 5.8: DVH-points for target structures, test = paired t-test between dCT_{CBCT} and ReCT, $\alpha \leq 0.05$

Patient ID		*PTV*			*CTV*		
		pCT	dCT_{CBCT}	ReCT	pCT	dCT_{CBCT}	ReCT
131	D_{50}	99.8	100.3	99.2	100.5	101.1	100.1
133		100.0	100.1	100.2	100.0	100.2	100.3
134		100.0	99.9	99.8	100.0	99.8	99.8
135		100.0	100.1	100.5	100.1	100.4	100.5
136		100.0	100.1	100.4	100.2	100.8	100.6
137		99.8	100.5	100.4	100.1	100.7	100.7
138		99.9	100.6	100.7	100.0	100.6	100.8
P-value				0.77			0.49
131	D_{95}	95.2	94.3	94.6	97.2	95.4	94.1
133		98.0	96.5	98.0	98.4	95.5	98.4
134		96.8	96.7	92.8	94.0	97.1	97.0
135		97.5	94.5	98.5	98.5	98.6	98.7
136		97.3	97.2	97.7	98.2	98.4	98.4
137		97.1	95.9	94.6	97.8	97.6	97.8
138		97.5	96.2	95.4	97.9	98.1	98.0
P-value				0.97			0.60
131	D_2	103.9	104.6	103.5	104.0	104.7	103.6
133		102.6	103.0	103.2	102.4	102.6	102.7
134		103.1	103.3	103.3	103.0	103.0	103.1
135		102.1	102.4	102.5	102.1	102.4	102.6
136		103.0	103.3	103.4	103.0	103.5	103.2
137		102.5	103.7	103.8	102.4	103.5	103.2
138		101.8	103.5	103.2	101.8	103.4	103.1
P-values				0.49			0.24

The DVH-point used for the parotid glands are D_{mean} and for the spinal cord, D_{max}. The dose constrains for these organs are $D_{mean} = 26$ Gy and $D_{max} = 45$ Gy [17].
When comparing the dose for dCT_{CBCT}- and the ReCT-based dose plan some difference is observed. The dose given the parotid dxt in Patient 136 exceeds the dose constrains for dCT_{CBCT}, however not for ReCT.
A paired t-test conducted to test for difference in mean between dCT_{CBCT} and ReCT, was found not significance. Thereby leading to no significant difference for mean values for the parotid glands (Table 5.9). However it should be noticed that even though no difference in mean was observed, some patients experienced dose exceeding the dose constrains in one dose plan but not the other.
The dose constrain of D_{max}=45 Gy for the spinal cord is fulfilled for every case except patient 137 at the ReCT scan (Table 5.9). A paired t-test found no difference in mean between dCT_{CBCT} and ReCT at a significance level of 0.05.

Table 5.9: DVH-points for OAR, test = paired t-test between dCT_{CBCT} and ReCT, $\alpha \leq 0.05$. Dose exceeding dose constrains marked with bold.

Patient ID	*Structure*	*pCT*	dCT_{CBCT}	*ReCT*
131	Parotid dxt	22.8	22.2	22.0
133		**57.1**	**58.9**	**61.2**
134		**38.6**	**40.6**	**44.4**
135		**30.1**	**31.1**	**28.7**
136		25.1	**29.9**	25.6
137		**32.0**	**33.7**	**27.3**
138		18.7	20.4	16.3
P-value				0.29
131	Parotid sin	24.2	22.1	23.1
133		24.3	22.3	25.5
134		**31.1**	**26.4**	**34.0**
135		18.8	21.1	16.1
136		**31.6**	**29.3**	**27.7**
137		**37.7**	**39.2**	**45.1**
138		24.9	25.0	22.1
P-value				0.29
131	Spinal Cord	41.5	42.1	41.5
133		41.8	41.2	41.7
134		43.1	43.2	43.6
135		38.7	40.3	39.5
136		44.4	43.6	33.1
137		43.2	43.0	**45.5**
138		44.6	44.4	43.3
P-value				0.42

5.2.2.2 Conformity results

Table 5.10: Volume for the 95% isodose structure, as well as CI_{95}, LCF_{95}, $NTOF_{95}$. Test = Wilcoxon rank sum between dCT_{CBCT} and ReCT, $\alpha \leq 0.05$

Patient ID		*pCT*	dCT_{CBCT}	*ReCT*		*pCT*	dCT_{CBCT}	*ReCT*
131	V_{95} [cm^3]	559.9	499.6	494.3	CI_{95}	0.92	1.0	0.49
133		479.3	427.6	430.0		1.2	1.2	1.2
134		290.6	296.4	300.1		1.3	1.3	1.9
135		208.3	210.6	211.8		1.3	1.3	1.5
136		194.0	181.7	181.5		1.2	1.2	1.8
137		321.8	299.2	298.6		1.2	1.2	1.2
138		203.6	212.8	211.4		1.3	1.4	1.5
P-value								0.11
131	LCF_{95}	0.87	0.86	0.81	$NTOF_{95}$	0.04	0.13	0.13
133		0.74	0.89	0.89		0.19	0.23	0.28
134		0.99	0.98	0.95		0.20	0.26	0.49
135		1.00	0.96	0.95		0.19	0.22	0.32
136		0.95	0.90	0.94		0.04	0.24	0.48
137		0.98	0.96	0.94		0.17	0.18	0.21
138		1.00	0.97	0.95		0.20	0.32	0.37
P-value				0.30				0.02

Dose calculation based on pCT and dCT obtains values around one, which is the ideal for CI (Section 4.3.2).
LCF is a measure for the coverage of the target and should, as for CI, ideally be one. Values of LCF for dCT_{CBCT} and ReCT are approximately of the same size for every patient. When values of LCF for dCT_{CBCT} and ReCT are equal it indicates similar target coverage, which is desirable.
The NTOF is optimal with a value of zero denoting, where no normal tissue is inside the 95% isodose. Variation of values for NTOF is observed between the patients and scans. The NTOF for $dCT_{CBCT}$and ReCT is found to be of nearly same size for four of seven patients. However large variation is observed for patient 134 and 136; where a large amount of normal tissue is found to be within the 95% isodose. Conducting a Wilcoxon rank sum test to evaluate if the variation between the values of dCT_{CBCT} and ReCT it is found that $NOTF_{95}$ obtains a significant difference in mean, whereas CI_{95} and LCF_{95} do not.

5.3 CBCT-based dose calculation

This chapter presents the results of dose calculation based on CBCT. The initial dose plan is transferred to CBCT with the structures of ReCT and dCT and compared to the dose plan on ReCT with manually delineated structures done by a physician. This is done to evaluate whether or not it is possible to perform dose calculation on CBCT even though the HU values are not correct (Figure

4.1C). To distinguish between the different scans with different structures a new notation is used - X_y.

- X: Symbolises the scan, either ReCT or CBCT
- y: Symbolises the origin of the structure set, either M or A
- M: Manually delineated structures
- D: Deformed structures, obtained by the DIR between pCT and CBCT.

As in the previous chapter three points on the DVH are found for the PTV and CTV; D_{50},D_{95} and D_2 (Table 5.11). Values are found to be of the same size for all DVH-points accordingly to the structure.
To test if the difference between the dose of $ReCT_M$, $CBCT_M$ and $CBCT_D$ is significant, an ANOVA has been conducted for PTV and CTV (Table 5.11). It is found that none of the DVH points are significantly different with a significance level of 0.05, thereby no difference in mean between $ReCT_M$, $CBCT_M$ and $CBCT_D$ can be detected.

Table 5.11: Dose endpoints for target volumes, Test = ANOVA, $\alpha \leq 0.5$

Patient ID		*PTV*			*CTV*		
		$ReCT_M$	$CBCT_M$	$CBCT_D$	$ReCT_M$	$CBCT_M$	$CBCT_A$
131	D_{50}	99.2	100.2	99.4	100.1	100.9	100.0
133		100.2	99.0	99.0	100.3	99.0	98.9
134		99.8	99.9	103.3	99.8	99.8	99.6
135		100.5	100.0	100.1	100.5	100.5	99.9
136		100.4	99.7	99.9	100.6	100.3	99.9
137		100.4	100.4	100.3	100.7	100.6	100.6
138		100.7	99.6	99.7	100.8	99.8	99.9
p-value				0.67			0.15
131	D_{95}	94.6	93.5	93.3	94.1	94.5	87.5
133		98.0	96.6	96.7	98.4	97.2	96.1
134		92.8	96.6	93.0	97.0	97.0	96.9
135		98.5	94.7	97.3	98.7	98.0	97.6
136		97.7	96.6	96.6	98.4	97.6	97.2
137		94.6	95.9	94.5	97.8	97.5	97.8
138		95.4	95.9	96.0	98.0	96.8	96.5
p-value				0.82			0.34
131	D_2	103.5	104.7	104.0	103.6	104.9	104.1
133		103.2	101.9	101.8	102.7	101.3	101.2
134		103.3	103.4	103.3	103.1	103.0	103.2
135		102.5	102.4	102.3	102.6	102.4	102.2
136		103.4	102.9	102.8	103.2	103.0	102.7
137		103.8	103.9	103.8	103.2	103.5	103.2
138		103.2	102.9	102.9	103.1	102.7	102.7
p-value				0.79			0.75

M:Structureset from ReCT - Manually delineated structures
D:Structureset from dCT_{CBCT} - deformed structures.

The DVH-point used for the parotid glands are D_{mean} and for the spinal cord, D_{max} (Table 5.12). Results similar to the one obtained in Chapter 2.2.3.1 are obtained for all OAR, except for patient 131, where the parotid sin for $CBCT_M$ exceeds the dose constrain. The dose obtained with the $ReCT_M$ and $CBCT_M$ dose plan are for many of the organs and patients very similar which is expected since these dose plans are based on the same structures. When the dose for $CBCT_M$ varies from $ReCT_M$, correlation with dose of $CBCT_D$ is found. This suggests a correlation with the modality used for the dose plan.
To test if the difference between the dose of $ReCT_M$, $CBCT_D$ and $CBCT_M$ is significant, an ANOVA has been conducted for all OAR (Table 5.12). It is found that none of the DVH points are significantly different when using a significance level(α) of 0.05, thereby no difference in mean between $ReCT_M$, $CBCT_M$ and $CBCT_D$ can be detected. However as previously stated the reader should notice that in some cases the dose exceeds the dose constrains using $CBCT_M$ or $CBCT_D$ but not with ReCT.
CI_{95} obtains higher values for $CBCT_M$ and $CBCT_D$ in patient 134 and 136 compared to $ReCT_M$ (Table 5.13). $CBCT_D$ have a higher value of CI_{95} than $ReCT_M$ for all patients except 131. For four of seven patient similar values of CI_{95} are found for $ReCT_M$, $CBCT_D$ and $CBCT_M$. Values of LCF_{95} are found to vary some for $CBCT_M$ and $CBCT_D$ and ReCT.
$CBCT_B$ gives values higher than $ReCT_M$ in $NOTF_{95}$ for all patients, indicating that more normal tissue receives high dosage. $CBCT_M$ gives higher values of $NOTF_{95}$ than $ReCT_M$ for six of seven patients.

Table 5.12: DVH-points for OAR. Bold symbolizes dose exceeding dose constrains, Test = ANOVA, $\alpha \leq 0.05$

Patient ID	*Structure*	$ReCT_M$	$CBCT_D$	$CBCT_M$
131	Parotid dxt	22.0	24.6	24.4
133		**61.2**	**58.5**	**60.0**
134		**44.4**	**40.7**	**44.8**
135		**28.7**	**31.0**	**29.4**
136		25.6	**29.8**	25.4
137		**27.3**	**33.9**	**27.3**
138		16.3	20.0	21.7
p-value				0.97
131	Parotid sin	23.1	25.4	**26.8**
133		25.5	22.1	24.9
134		**34.0**	**26.3**	**34.3**
135		16.1	20.9	15.2
136		**27.7**	**28.8**	**27.6**
137		**45.1**	**39.4**	**45.1**
138		22.1	24.5	23.1
p-value				0.94
131	Spinal Cord	41.5	43.2	41.6
133		41.7	43.0	43.4
134		43.6	44.5	43.8
135		39.5	40.2	39.3
136		33.1	42.8	43.4
137		**45.5**	43.5	**45.5**
138		43.3	43.7	42.7
p-value				0.40

M:Structures from ReCT - Structures delineated by physician.
D:Structures from dCT_{CBCT} - deformed structures.

Table 5.13: Conformity Indices, Test = ANOVA, $\alpha \leq 0.05$

Patient ID	*Structure*	$ReCT_M$	$CBCT_D$	$CBCT_M$
131	CI_{95}	0.49	0.94	0.92
133		1.2	1.2	1.2
134		1.9	1.9	1.8
135		1.5	1.5	1.5
136		1.8	1.9	1.8
137		1.2	1.2	1.2
138		1.5	1.5	1.4
p-value				0.59
131	LCF_{95}	0.81	0.81	0.79
133		0.89	0.89	0.88
134		0.95	0.95	0.94
135		0.95	0.81	1.0
136		0.94	0.94	0.93
137		0.94	0.94	0.93
138		0.95	0.95	0.97
p-value				0.98
131	$NTOF_{95}$	0.13	0.13	0.13
133		0.13	0.28	0.28
134		0.49	0.49	0.47
135		0.32	0.46	0.30
136		0.48	0.48	0.46
137		0.21	0.21	0.19
138		0.31	0.37	0.31
p-value				0.19

M:Structures from ReCT - Manually delineated structures
D:Structures from dCT_{CBCT} - deformed structures.

Evaluation of dose distribution based on a deformed image set and a CBCT has been conducted. Dose distribution is derived based on dCT_{CBCT}, CBCT and ReCT all with deformed structures from dCT_{CBCT}. Average DVH-points are determined as well as the percentage wise deviation from ReCT (Table 5.14)[2]. From evaluation of the average DVH points it is not possible to determine if dose calculation based on dCT_{CBCT} performs better or worse than dose calculation based on CBCT.

Table 5.14: Average DVH points and percentage wise deviation from $ReCT_D$ for $dCT_{CBCT(D)}$ and $CBCT_D$. Dose calculation based on dCT_{CBCT}, CBCT and ReCT all with deformed structures from dCT_{CBCT}

	$dCT_{CBCT(D)}$	$ReCT_D$	$CBCT_D$	% $dCT_{CBCT(D)}$	% $CBCT_D$
PTV					
D_{50}	100.3	100.0	100.0	0.3	0.0
D_{95}	95.8	96.1	95.5	-0.3	0.6
D_2	103.5	103.0	103.4	-0.4	0.3
CTV					
D_{50}	100.6	100.5	100.3	0.1	-0.2
D_{95}	97.5	97.8	97.0	-0.3	-0.9
D_2	103.4	103.6	103.4	-0.2	-0.2
Parotid dxt	29.7	30.6	30.0	-2.9	-0.2
Parotid sin	27.2	26.2	27.6	-3.8	5.34
Spinal Cord	42.8	43.2	43.0	-0.9	0.5

[2]Based on six patients. Patient 133 is excluded due to technical problems with the TPS

Chapter 6

Discussion

In this chapter we will discuss the results obtained with the use of DIR. Initially the limitation of the DIR will be presented.
Discussion will initially be in regards to the DIR based on CBCT and ReCT. The main focus of this chapter will be on the DIR based on CBCT compared to ReCT. This concerns the dosimetric and geometric evaluation. Finally discussion of CBCT based dose calculation will be presented.

6.1 Limitation of the DIR

During this study, two clear limitations of the DIR have been found; smaller FOV for CBCT than for regular CT, and differences in the HU values of CBCT and CT.
The image acquisition of CBCT leads to a smaller FOV than regular CT. This will become a problem if the delineated structures are not included in the CBCT. CBCT will be the decisive factor for the VOI, wherein the DIR will perform. Clinical relevant information of the CT not included in the VOI will therefore not be reflected in the deformed image. In some cases the tumour will be too large to be included in the FOV of CBCT, hence DIR of CBCT-CT cannot be used.

A challenge in using CBCT in DIR is the large amount of artefacts of this image modality. Ueda et al. [45] have performed a study evaluating the impact of artifacts of CBCT on DIR algorithms. The study was performed on several *H&N* cancer patients and DIR between CT and CBCT. Ueda et al. observed, the noise in CBCT only has little effect on the registration accuracy when used as base for DIR. Additionally was found that a large shift in the HU-values causes errors, which was also observed in present study. Figure 6.1 visualises two different patients, both with a CBCT, pCT and the corresponding $\mathrm{dCT}_{\mathrm{CBCT}}$ within a HU-window of 300 to 600. The intensity of CBCT in Figure 6.1(b) is very different from the other images leading to an error in the $\mathrm{dCT}_{\mathrm{CBCT}}$. Inspection of dCT shows enlarged and blurred edges of the columnar and removal of the skull, which is black in this patient. For comparison, Figure 6.1(a) is an example of similar HU units in pCT and CBCT and a good result of the DIR. The edge in the back of the patient (a) is due to limited FOV. The error of the DIR rise from the algorithm used, which is intensity based. Large difference in intensity of the registered images will thereby cause errors.

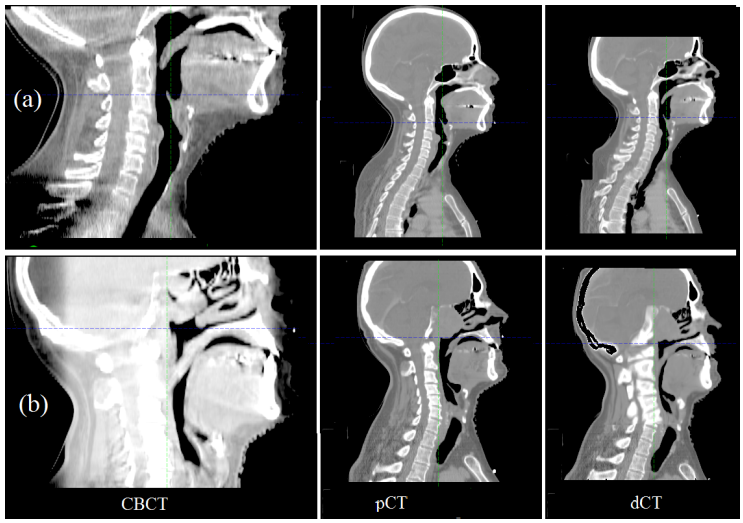

Figure 6.1: CBCT, pCT and dCT for two patients, *(a)* and *(b)*. The same values of HU (300-600) are displayed for all images, to visualize the intensity in CBCT which for *(b)* patient is very different. *(a)*: Patient 131 *(b)*: Patient excluded from this study due to error caused by difference in HU

6.2 Deformable image registration based on CBCT and ReCT

In this section discussion regards the comparison of DIR based on a CT scan and a CBCT scan.
Geometrical similarities are observed between dCT_{CBCT} and dCT_{ReCT} for the target structures (GTV, CTV and PTV) and for parotid glands. The small variation between the structures could be caused by a registration error. The volume of the spinal cord is estimated to be larger when using dCT_{ReCT} compared to the volume estimated by dCT_{CBCT} which leads to large differences. For the spinal cord, the mean values of DSC for dCT_{CBCT} and dCT_{ReCT} are found to be significantly different.
The difference between dCT_{CBCT} and dCT_{ReCT} suggest that the algorithm depend on the modality used as base for the DIR. This could be caused by the larger similarities of the image intensity between pCT and ReCT compared to between pCT and CBCT. All structures, with exception of the spinal cord, show large similarity, and further comparison were performed between dCT_{CBCT} and ReCT as discussed below (Section 6.3).

6.3 Comparison of ReCT and dCT_{CBCT}

Geometric comparison

The strength of this study, compared to previous studies is the existence of a CT scan representing the ground truth. This CT scan has been provided with structures delineated by a physician, and represent how the structures would have been delineated if the patient received a manually adapted treatment plan. This makes it possible to compare the obtained results of the DIR to what would be defined as the ground truth.

The propagated structures are, in this study, evaluated using selected geometrical measures. These measures all have their limitations as discussed in section 4.3. However combination of the chosen geometrical measures should provide a good overall interpretation.

Variations are observed for all geometrical measures for GTV, even if patient 134 is ignored. The GTV is inferior compared to the the PTV. GTV is, for every patient in this study placed close to the trachea which is not consistent in size and shape between the two scans (Figure 6.3) The difference arises due

to the patient having more or less free airways. The delineation of GTV should

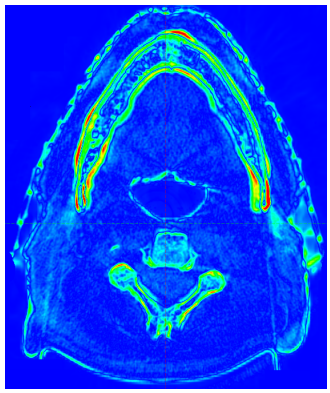

Figure 6.2: Difference between dCT_{CBCT} and CBCT. It is observed that the trachea is similar in these images, which is also expected since dCT_{CBCT} originates from CBCT. Patient ID: 136

not include any air cavities. Manually delineation of GTV performed on pCT will be at the edge of trachea. This also is the case in the deformed image due to the intensity based algorithm used in the DIR. The shape of GTV will, however match the shape of trachea in the CBCT due to dCT_{CBCT} containing the structural information from CBCT. Figure 6.2 show the difference between CBCT dCT_{CBCT} illustrating the size and shape of trachea are similar, leading to the shape of the deformed GTV being dependent on the shape of trachea in CBCT. Because of differences in the size and shape of trachea on the CBCT and ReCT, the manual and deformed GTV will not be alike as seen in Figure 6.3.
The PTV and CTV are found to match the structure of ReCT nicely, both in estimated volume, COM, DSC and OI. However PTV and CTV should be independent of the deformation due to the origin of these structures. CTV and PTV are margins added by the physician, based on preliminary knowledge. The delineation of these structures is therefore not based on the intensities of the image. Ideally only GTV should be deformed and subsequently the CTV and PTV should be manually delineated. By adding the CTV and PTV subsequent a change in the size and shape of these structure might arise. However to investigate the difference in using deformed structures of CTV and PTV compared to manually delineated CTV and PTV based on deformed GTV, was beyond the scope of this study.

Hou et al. obtains an average DSC for GTV at 0.76 which is a bit higher than the one obtained in this study (DSC=0.66) [29] . Hou et al. however compares the deformed structure with a structure manually delineated at the CBCT.

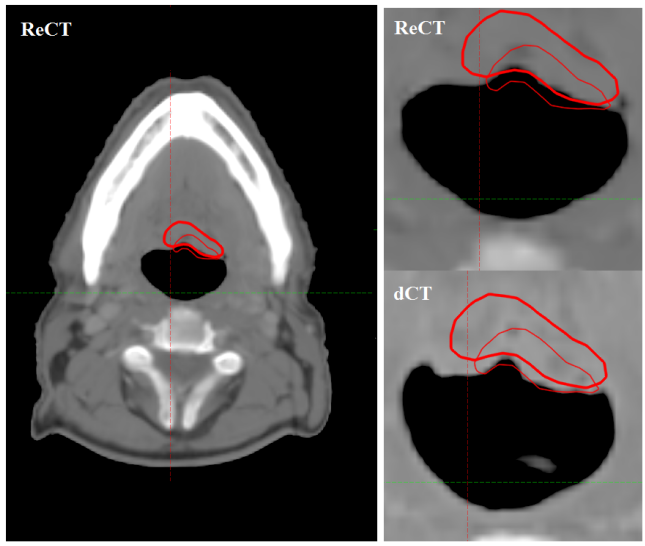

Figure 6.3: GTV on ReCT and dCT_{CBCT}. Illustration of the placement of trachea with respect to GTV. Bold structures represent GTV from ReCT. Left: Extraction of trachea. Patient ID: 136

Delineation on CBCT is prone to some uncertainty due to the low contrast. Furthermore the trachea is identical in the two images since the deformed image is based on the CBCT which the manual delineation has been performed on. This will eliminate the uncertainty of different size and shape in the trachea and lead to a higher value of DSC.
Tsuji et al. who perform CT-CT registration, obtains an average value of 0.69 for DSC of GTV (Table 5.6) [44]. The deformed structures are based on CT acquired at mid-treatment and compared to pCT. This set up is similar to the set up used in this thesis and the value of DSC is closer to the one obtained in our study. Values of OI are found to be similar as well. Due to the value of DSC and OI for GTV being similar to the results in this study an indication of CBCT as base for image registration being as good as DIR using CT is observed.

The relative volume of ReCT and dCT_{CBCT} with respect to pCT for all target structures show no significant difference in mean. Values of COM, DSC and OI for GTV obtains reasonable results. Generally the use of DIR propose a reasonable tool for use in adaptive radiation therapy with regard to GTV. However certain reservations should be made with regard to instances described above.
The propagation of the spinal cord structure shows large COM and low values of DSC and OI. Large percentage-wise differences for dCT_{CBCT} with respect to ReCT is found in six of the seven patients. This indicates that the structure

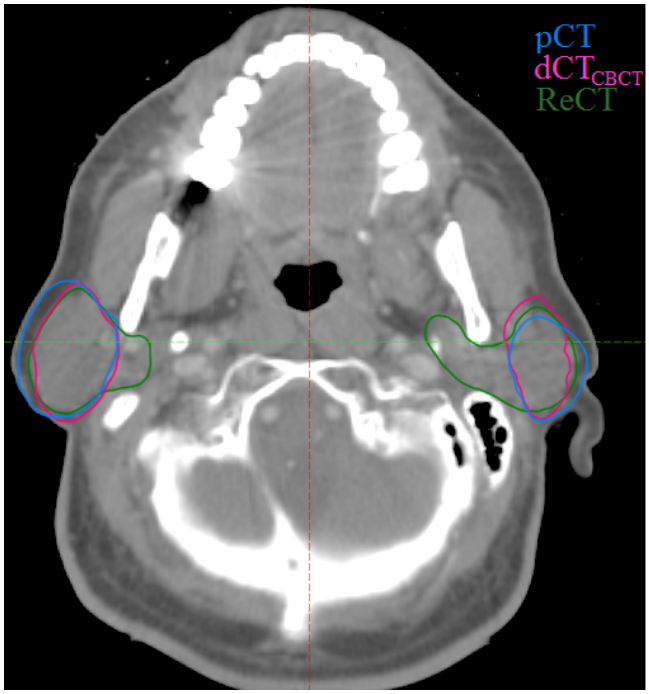

Figure 6.4: Parotid gland on ReCT. Illustrating the delineated and propagated parotid glands. Patient ID: 135

defined by the DIR is not usable for adaptive radiation therapy. The spinal cord is, however, an organ that is fairly easy to delineate manually or by the use of model based-delineation.

The structures of the parotid glands reveals that the DIR estimates the volume to be smaller than the manually delineation, in nearly every case. As seen in Figure 6.4 the parotid glands are estimated differently in shape by the physician and the DIR. The deformed structures are very similar to the one of pCT; however the manually delineated structures of ReCT are very different in shape. The manually delineation of the parotid glands on ReCT, is performed in this way for all patients. The delineation on the ReCT account for the deep part of the parotid glands, which was not done on the initial pCT. This gives rise to the large variation in used geometrical measures between ReCT and dCT_{CBCT}. It is important to emphasise that none of the manual delineations of parotids glands are falsely obtained[1]. The difference arises from different delineation approaches by of the different physicians. By visual inspection of the parotid glands, it is found that by ignoring the deep part of the parotid glands, as done in pCT, the structures of ReCT and dCT_{CBCT} are much alike (Figure 6.4). Our study obtains values of DSC for the parotid glands, comparable to the one obtained by Tsuji et al. [44]. Values of OI are found lower than Tsuji et al. Variation in the delineation could have caused this.

Some of the variation in the geometrical results could, as discussed above be related to the manual delineation of the structures. Structures in pCT and ReCT are not delineated by the same physician, and are thereby prone to some variation.
Chao et al.[14] made use of a DIR to reduce variation of delineation in *H&N* cancer patients. This DIR was based on a reference template and the structures were deformed to match the actual image. Physicians were asked to delineate from scratch and with assistance from the deformed structures. Chao et al. found that by using the deformed structures to assist the delineation the variation, as well as time spend on delineation, was reduced noticeable. This opens up for possibilities of using the deformed structures in adaptive radiation therapy. This method improves the precision but does however not give information about the accuracy.

Variations observed for the parotid glands are found to be influenced by delineation performed by different physicians. Visual inspection of the parotid glands show considerable similarity if the deep part of parotid gland is ignored. This indicates that the DIR is usable for estimating the structures of the parotid glands. However some sort of standardisation of the way delineation of these

[1] Delineated structures on pCT and ReCT was re-confirmed by the physician, Christian Maare

structures is done should be set up.

Dosimetric comparison

The measures used above for comparison of structures only provide a geometrical evaluation. A dosimetric comparison is performed, to obtain information regarding the provided dose using the deformed image and structures. This will give information about if the variability in the structures has any influence on the provided dose.

The dosimetric comparison reveals that no significant difference can be observed with regard to the DVH-point. Table 5.8 shows that the provided dose are similar in pCT, ReCT and dCT_{CBCT}. This indicates that the initial treatment plan is very robust to changes and the tumour control is not at risk. The DVH-points for the OAR also reveals no significant difference in mean between the dose based on ReCT and dCT_{CBCT}. However the dose for parotid dxt, exceed the dose constrains for four of seven patients at pCT and dCT_{CBCT} (Table 5.9). This is due to the placement of tumour tissue. During optimization of the treatment plan it is a priority for the physicist/dosimetrist to foremost secure tumour control. By comparing the dose to parotid dxt it is found that when the parotid gland in the one side receive dose that exceed the dose constrains, the gland in the other side will be below the dose constrain, with exception of Patient 137. This is an intentional choice from the physicist/dosimetrist during the optimization of the treatment plan, since this will ensure some function of at least one of the glands, leading to enhanced quality of life for the patient. The dose calculation based on ReCT gives are used for dosimetric comparison to dose based on dCT_{CBCT}, however it can also be used to evaluate the dose provided by not replanning. Comparing DVH-points for pCT and ReCT no noticeable difference is observed for PTV and CTV. For the parotid glands are an increase in dose for ReCT compared to pCT observed for some of the patients. This indicates these patients might would benefit from replanning. However no patients exceeds the dose constrain in ReCT where it is not also exceeded in pCT.
The dose constrain for the spinal cord is exceeded in ReCT for one patient (137). This suggests that replanning of the treatment plan should be performed to ensure sparing of the organs at risk. By replanning, a new treatment plan will be optimized to the actual delineated structures. Replanning was not conducted as part of this study, since it was not within the scope. By using the same treatment plan in all three cases is it possible to evaluate the impact of not replanning.

The use of DVH-points however also have some drawbacks. The provided dose

is three-dimensional and collected to the two-dimensional measure, DVH. The use of DVH points does not take the shape of the DVH curve into consideration. This means that large variations between the shapes of the DVH, might not be reflected in the selected DVH point. This is especially an issue for the OAR, since the shape of the DVH-curve normally varies a bit for these structures.

Values of CI_{95} and LCF_{95} obtains similar results for pCT, ReCT and dCT_{CBCT}. Values of LCF_{95} and CI_{95} shows no significant difference in mean between ReCT and dCT_{CBCT}. Values of $NTOF_{95}$ are found to show significant difference in mean, indicating difference between ReCT and dCT_{CBCT}. For patient 134, 135 and 136 values of ReCT are much larger than for pCT and dCT_{CBCT}. This arises from the volume of PTV being estimated smaller in ReCT than in pCT and dCT_{CBCT} for these patients (Table 5.5).
Delineation of patient 134 showed a large difference in the size and placement of GTV, CTV and PTV. This give rise to a value of 0.49 for ReCT due to the large difference in size of V_{95} and V_{PTV}. Confirmation done by physician identified the delineation for pCT and ReCT to be correct.
For every patient the $NTOF_{95}$ is found to be larger for ReCT than for pCT. This suggests that by not replanning the surrounding normal tissue will be exposed to an increased dose. This is comparable to other studies suggesting that by replanning, the only benefit will be with regard to the normal tissue and OAR. Likewise it is found that replanning only profit selected patients who will benefit significantly of a new treatment plan [21, 9]. This is expected, due to the geometry of the tumour and the robust field set-up. The tumours are placed centrally and when the patient and tumour shrinks the lateral OAR will move int a high dose area.

Even though some geometrical variation is observed between the structures, little effect on the dosimetric outcome is observed.
The results of DIR between pCT and CBCT represent a promising tool for adaptive radiation therapy, but do however give rise to unanswered questions. The image produced by the DIR is not the truth since it has not been produced by an actual scan but a computer program. Therefore the image should be interpreted with some consideration. A solution could be to transfer the deformed structure to a CBCT image set and get manual adjustment from a physician. This procedure however demands the ability to perform dose calculation on CBCT.

6.4 CBCT-based dose calculation

Dose calculation based on CBCT has been conducted and compared to dose based on ReCT. No significant difference in mean is observed between $CBCT_M$,

$CBCT_D$ and $ReCT_M$ which indicates that the dose obtained using CBCT is comparable to the one obtained using ReCT. This is the case for both target structures and OAR.

Several other studies obtain similar results, however other studies have performed HU calibration [20, 51, 30]. This is performed to ensure relation between HU-values and electron density. This was not performed in this study prior due to time constrains.

Even though this study reveals no significant difference between dose calculation on ReCT and CBCT, it is not recommended to ignore pre-processing of CBCT prior to dose calculation. CBCT images are known to be prone for containing artefacts and errors/variation in HU. Further studies should therefore be conducted to obtain the most correct and efficient way to pre-process CBCT images for dose-calculation.

In addition this study compares the use of CT, deformed CT and CBCT as a base for dose calculation to evaluate the difference in obtained dose (Table 5.14). Small differences in the obtained values were observed, however no tendency towards which dose calculation was most correct was found. Investigation was only performed on six patients. This is a small group and investigation performed on a larger foundation might give a more unequivocal result.

Chapter 7

Conclusion

The performance of an available DIR has been evaluated with regard to geometric and dosimetric measures. The evaluation was based on DIR between the pCT and a midterm CBCT compared to manually delineation of structures on ReCT conducted at the same time as the CBCT. ReCT served as the ground truth. Additionally was DIR based on CT and CBCT compared to evaluate if the algorithm is dependent on the modality used. Dose calculation based on CBCT was likewise evaluated.

It was found that DIR based on CBCT can be used on equal terms as CT. Additionally was found that similar results was obtained by CBCT-based dose calculation compared to based on CT. This indicates that CBCT-based dose calculation has potential for use in adaptive radiation therapy.

Reasonable results were obtained for the geometrical measures with regard to the target- and parotid gland structures, however with some variation. The variation was for the GTV found to be influenced by the shape and size of the trachea. Additionally, different delineation approaches of the parotid glands was found to have an impact on the variation.
The geometrical measures for the spinal cord indicated that the DIR was not usable for this organ.

Even though some geometrical variation was observed for the structures, there

was a limited effect on the dosimetric outcome. The dosimetric comparison revealed no significant difference with regard to the DVH-point for all structures. Values of CI_{95} and LCF_{95} obtained similar results for pCT, ReCT and dCT_{CBCT}. This demonstrated that the conducted treatment plans were robust to anatomical changes. Values of $NTOF_{95}$ revealed significant difference between pCT, ReCT and dCT_{CBCT}, indicating that replanning is needed for sparring of the normal tissues. Generally the DIR was found as a promising tool for use in adaptive radiation therapy with regard to the target structures and the parotid glands.

Chapter 8

Future work

This thesis finds DIR as a promising tool for adaptive radiation therapy with regard to adaptation of the delineated structures. However, further work is necessary before implementation as a treatment standard can be done.
Directly derived from this thesis future work could include comparison of manually delineated CTV and PTV based on a deform GTV with manually delineation of these structures.
An issue with delineation of structures have been found in this thesis. Different delineation approaches of the parotid glands were found to have an impact on the variation between deformed structures and manually delineated structures. By visual inspection of the parotid glands, it was found that by ignoring the deep part of the parotid glands, as done in pCT, the structures of ReCT and dCT_{CBCT} was much alike. This indicates that interobserver variation has an impact on how well deformed structures match the manually delineated ones. It could be interesting in a future study to evaluate if the inter- and intraobserver variation is of same size as variation between deformed and manually delineated structures. The dosimetric comparisons performed in this study are based on DVH-points and treatment plan conformity. To further investigate the difference between the provided dose of ReCT- and dCT_{CBCT}-based dose calculation, NTCP and TCP could be evaluated. These are biological models providing the probability of tumour control and normal tissue complications. This can be used to evaluate the difference between use of treatment plans based on pCT, ReCT and dCT_{CBCT}.

CBCT-based dose calculation would as the use of deformable CT propose a tool for adaptive radiation therapy. The deformed CT image set is based on a computer algorithm and differences to the actual can occur, therefore the use of CBCT present a feasible tool. However as described, does HU on CBCT differ from HU on CT, and dose calculation may not be correct. Present study indicate that dose calculation is possible, however further investigations and procedures for data acquisition should be conducted.
The above stated subjects for future work are among many studies performed before use of DIR in adaptive radiation therapy can be used.

Appendix A

Abstract - Accepted for poster presentation at ESTRO 31, 2012

R.B. Eiland, C.F. Behrens, D. Sjöström, C. Maare, R.R. Paulsen, E. Samsoe

Purpose

Anatomical changes can occur during RT treatment of *H&N* cancer patients. This can lead to a difference in planned- and delivered dose. Adaptive RT has the potential to overcome this, utilizing deformable image registration (DIR). The purpose of the study was to evaluate the performance of a DIR algorithm, using geometric and dosimetric measures.

Materials

Seven patients treated with IMRT were included in this study, each with a planning- and midterm CT (pCT, ReCT) as well as a CBCT acquired on the same day as the ReCT. ReCT served as the ground truth for evaluation of

the DIR. A deformed CT (dCT) with contours was created by deforming the pCT and associated manually drawn contours to the CBCT. A commercial software package using the Demons DIR algorithm (SmartAdapt, Varian Medical Systems, v.11.0) was utilized. The geometrical comparison were based on the estimated volumes from the contours on the dCT, and the manually drawn contours on the ReCT. Center of mass shift (CMS) and dice similarity coefficient (DSC) were found between contours on dCT and ReCT. In the treatment planning system (Eclipse, Varian Medical system, v.10.0) the initial treatment plan was copied to the dCT and ReCT and the dose recalculated. DVH points (D50 for parotid glands and Dmax for spinal cord) were evaluated. Conformity index (CI), lesion coverage fraction (LCF) and normal tissue overdose fraction (NTOF) was evaluated with regard to target coverage.

Results

The PTV volume was estimated larger for dCT than ReCT with a median of 4.9% (range,-4.0; 69.3). Four of seven patients obtained a volume difference of $<$5%. Six patients had a median CMS for PTV of 0.28 cm (range, 0.05; 0.43). The median DSC was 0.88 (range, 0.60; 0.95). Similar results were obtained for GTV and CTV. The median relative volume deviation from ReCT was -10.7% (range, -28.0; 16.7), 21.8% (range, -42.1; 3.4) and -6.0% (range, -33.1; 32.3) for parotid dxt, parotid sin and spinal cord, respectively. The median CMS was 0.51 cm (range, 0.19; 2.22). DSC ranged from 0.45 to 0.85. The median relative deviation from ReCT in DVH points for parotid dxt, parotid sin and spinal cord was 8.3% (range, -8.4; 25.3), -12.7% (range,-28.6; 31.0), and 1.3%(range,-5.4; 31.8), respectively. CI, LCF and NTOF are visualized in the figure. Ideal values of CI and LCF are unity and zero for NTOF.

Conclusion

The DIR produced geometrical results similar to the ReCT in four of seven patients with regard to the target. Larger geometrical variations were observed for organs at risk (OAR). OAR contours obtained with the DIR were for nearly all patients estimated smaller than in the ReCT whereas target contours were estimated larger. The dosimetric results for OAR showed some variation between dCT and ReCT, especially for the parotid glands. The LCF were similar for dCT and ReCT, whereas NTOF were larger for ReCT than for dCT. Despite variation in volume and dose, between dCT and ReCT, the differences were within acceptable limits for most of the patients.

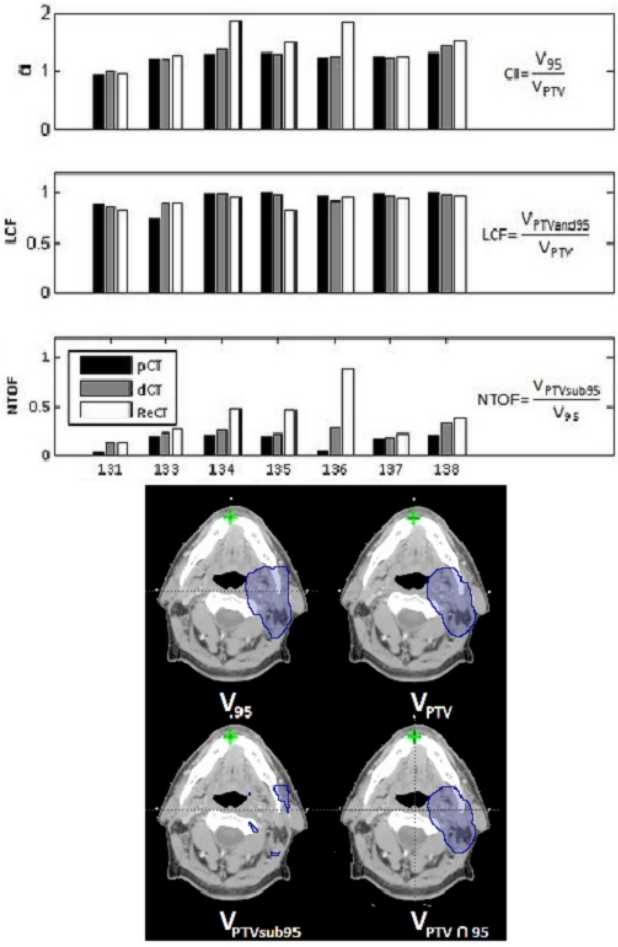
CII
LCF
NTOF
pCT
dCT
ReCT
131
133
134
135
136
137
138
$CII = \frac{V_{95}}{V_{PTV}}$
$LCF = \frac{V_{PTVand95}}{V_{PTV}}$
$NTOF = \frac{V_{PTVsub95}}{V_{95}}$
V_{95}
V_{PTV}
$V_{PTVsub95}$
$V_{PTV \cap 95}$

Figure A.1

Appendix B

Poster presented at Department for Mathematical Modelling (IMM) at the Technical University of Denmark (DTU)

Herlev Hospital

Adaptive Radiation Therapy

Technical University of Denmark DTU

By Rikke Busch Eiland. Supervisors: Medical physicists Claus Behrens, Ph.D, Herlev hospital. Associate Professor Rasmus Paulsen, Ph.D. IMM -DTU

1. Introduction

Cancer in the head and neck area can be treated with radiation therapy, but the use of this will give rise to some challenges due to many important organs.
During treatment the size of the tumor can change drastically and affect the anatomy in the treated area. This could potentially mean that healthy tissue gets unnecessary irradiated, or that the tumor is not receiving enough radiation.

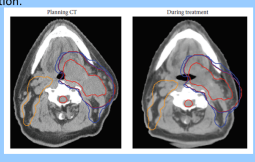

Currently the plan can be adapted to the new anatomy by conducting a new CT scan and manually delineating contours. This makes the treatment planning is a time consuming process, since it involve a physicist and a physician and must be conducted within 24 hours.
To evaluate the anatomical changes a cone beam computed tomography (CBCT) scan is performed halfway in the treatment course.

2. Problem statement

The aim of this study is to find a method to determine if it is necessary to conduct a new CT scan to adapt the treatment plan. This is performed by deformable registration between the original CT and a midterm CBCT. The result is a deformed CT depicting the actual anatomy. In this study a new CT scan has been conducted at the same time as the CBCT, and will be used as an expression of the truth.

3. Patient Data

The data consist of a planning CT (pCT), a CBCT, and a replanning CT (ReCT) as well as treatment plans for three patients with head and neck cancer. The data originates from patients that have experienced large anatomical changes during their treatment courses.

4. Data processing

Using a commercially available software (SmartAdapt, v.11 Varian), the pCT is deformable registered to CBCT. Deformable registration is based on the "demons algorithm". Contours from the initial pCT is also deformed to the mid-treatment CT for each patient, and propagated to the deformable registered CT image set (dCT).

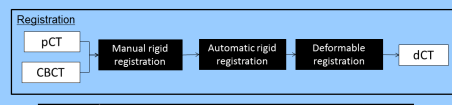

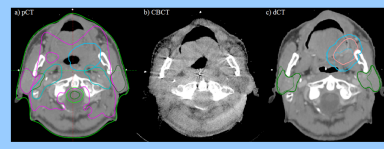

The dCT and ReCT is compared in two ways: geometric and dosimetric. Geometric to ensure the structures are delineated and propagated correctly, and dosimetric to evaluate the dose coverage of the target and organs at risk, see figure:

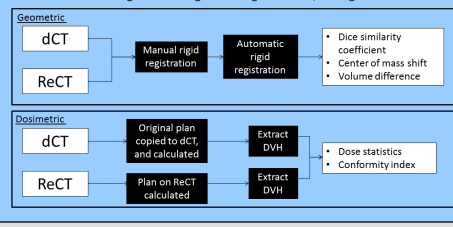

5. Results

Geometric:

In order to compare the propagated deformed structures, the volume for selected structures is found and the center of mass shift, and Dice similarity coefficient(DSC) between dCT and ReCT is determined, see figure below.

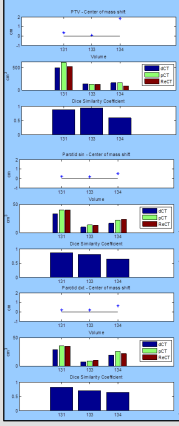

Center of mass shift and DSC is measures giving information about the placement and shape of the structure. The volume gives information about the size of the structure.

Center of mass shift, volume and DSC is determined for 3 patients for 3 structures. It is seen that the largest difference in the measures is seen in patient 134, and smallest for patient 133.

Patient	Structure	dCT	pCT	ReCT	Dsc	Center of mass shift
131	CTV	313,00	409,5	331,7	0,85	0,32
133	CTV	63,70	65,80	65,40	0,71	0,23
134	CTV	80,1	89,5	47,5	0,54	1,76
131	GVT	96,90	159,90	108,30	0,72	0,39
133	GTV	3,20	3,80	3,60	0,90	0,07
134	GTV	15,70	18,10	5,80	0,33	1,63
131	PTV	495,90	608,90	523,80	0,88	0,33
133	PTV	134,50	128,00	127,30	0,95	0,08
134	PTV	159,50	163,60	94,20	0,60	1,83
131	Parotid dxt	28,60	35,20	34,50	0,82	0,16
133	Parotid dxt	7,20	8,40	10,00	0,71	0,19
134	Parotid dxt	19	26,10	21,40	0,65	0,63
131	Parotid sin	33,50	40,00	39,70	0,87	0,22
133	Parotid sin	10,00	13,70	13,00	0,81	0,18
134	Parotid sin	16,80	22,20	23,60	0,65	0,51

Dosimetric:

To determine if it is possible to use the dCT for treatment planning, the Dose volume histogram (DVH) is examined and the conformity index is determined.
The DVH is examined to evaluate if there is a difference between the dCT and ReCT. Below the DVH for the structure PTV is depicted for two patients. It is seen that the shape of the DVH is close for patient 133, but varies a bit for patient 134

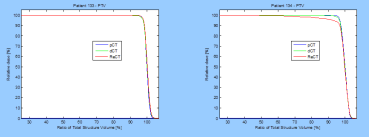

The Conformity index is evaluated to determine how well the target is covered by the planed dose. The conformity indices must be combined to determine the level of conformity. 3 measures is used.

Along with the plain conformity index, lesion coverage fraction (LCF) and normal tissue overdose fraction (NTOF) is determined. The optimal LCF is unity, and zero for NTOF. It is seen that the plan for patient 134 performers the best with regard to target coverage, but worst in case of sparing the normal tissue.

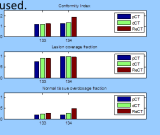

Figure B.1

Appendix C

Additional Results

Results form DIR based on ReCT and CBCT

Table C.1: Volume of OAR in cm^3

Patient ID	*Parotid dxt*		*Parotid sin*		*Spinal cord*	
	dCT_{CBCT}	dCT_{ReCT}	dCT_{CBCT}	dCT_{ReCT}	dCT_{CBCT}	dCT_{ReCT}
131	27.6	38.3	31.9	41.0	20.9	25.9
133	7.4	6.7	10.0	11.9	10.5	20.5
134	19.0	22.4	16.8	18.6	17.2	15.4
135	22.9	24.8	19.6	19.6	15.3	18.2
136	16.1	20.7	15.4	17.6	18.2	16.8
137	26.1	28.5	22.6	24.5	11.4	17.1
138	25.1	27.1	19.5	21.1	17.4	21.8

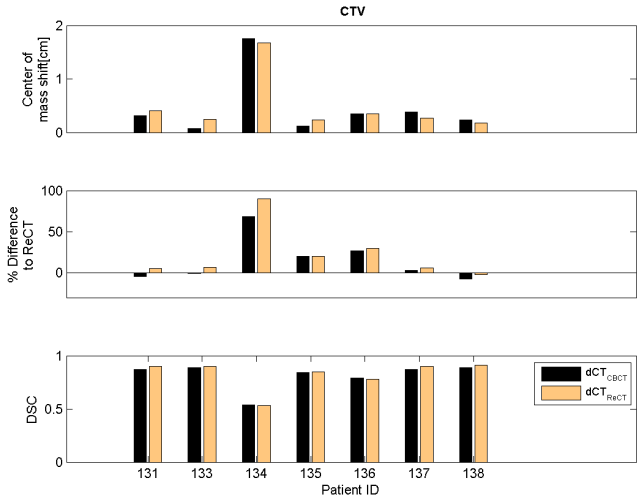

Figure C.1: CTV. Geometrical comparison between $\mathrm{dCT_{CBCT}}$ and $\mathrm{dCT_{ReCT}}$ relative to ReCT. *Top*: Center of mass shift *Middle*: Percentage wise deviation in volume of to ReCT. *Bottom*: DSC

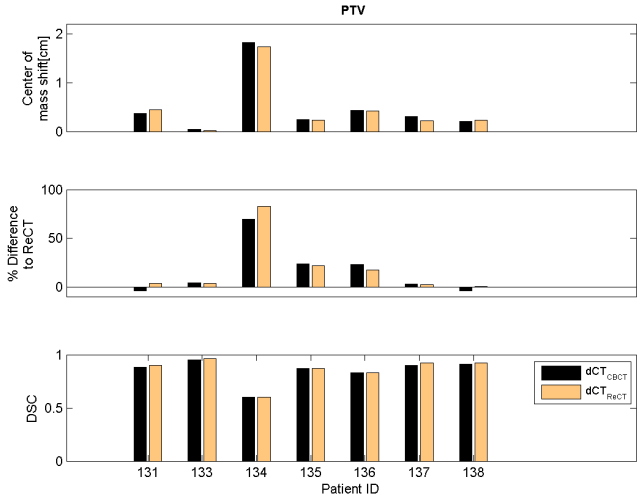

Figure C.2: PTV. Geometrical comparison between $\mathrm{dCT_{CBCT}}$ and $\mathrm{dCT_{ReCT}}$ relative to ReCT. *Top*: Center of mass shift *Middle*: Percentage wise deviation in volume of to ReCT. *Bottom*: DSC

Results form DIR based CBCT compared to ReCT

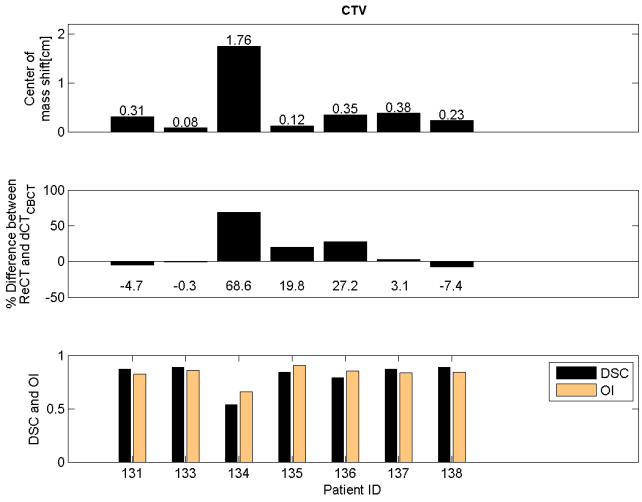

Figure C.3: Geometrical measures for CTV. *Top*: Center of mass shift between ReCT and dCT_{CBCT}. *Middle*: The volume of pCT, dCT_{CBCT} and ReCT relative to pCT. *Bottom*: DSC and OI determined between dCT_{CBCT} and ReCT

Table C.2: Volume of CTV

Patient ID	*Volume* $[cm^3]$		
	pCT	dCT_{CBCT}	ReCT
131	409.5	316.1	331.7
133	65.8	65.2	65.4
134	89.5	80.1	47.5
135	42.4	47.7	39.8
136	41.8	34.1	26.8
137	140.6	132.5	1285
138	79.1	72.5	78.3

Table C.3: Volume of Spinal cord

Patient	*Volume* $[cm^3]$		
	pCT	dCT_{CBCT}	ReCT
131	21.8	20.9	15.8
133	13.4	10.5	15.7
134	19.4	17.2	19.3
135	15.5	15.3	12.7
136	22.8	18.2	22.8
137	15.1	11.4	16.0
138	18.9	17.4	17.7

Bibliography

[1] http://www.varian.com/us/oncology/radiation_oncology/clinac/.

[2] http://scientificsentence.net/Radiations/images/attenuation_coefficients.jpg.

[3] http://www.varian.com/media/oncology/products/clinac/images/clinac_ix.jpg.

[4] http://www.dahanca.dk/get_media_file.php?mediaid=215.

[5] http://www.medicalphysics.org/apps/medicalphysicsedit/VANDYKCH08.pdf.

[6] http://server.elektro.dtu.dk/personal/jw/webbook/X-ray/Ct/main.pdf.

[7] http://ingenium.home.xs4all.nl/dicom.html.

[8] http://www.r-project.org/.

[9] http://medicalphysicsweb.org/cws/article/research/47050.

[10] Marianne Aznar. Lectureslides from course: Medical use of ionizing irradiation, 2010.

[11] J.L. Barker, A.S. Garden, K.K. Ang, J.C. O'Daniel, H. Wang, W.H. Morrison, D.I. Rosenthal, KS Chao, S.L. Tucker, R. Mohan, et al. Quantification of volumetric and geometric changes occurring during fractionated radiotherapy for head-and-neck cancer using an integrated CT/linear accelerator system. *International Journal of Radiation Oncology* Biology* Physics*, 59(4):960–970, 2004.

[12] J.T. Bushberg. *The essential physics of medical imaging.* Williams & Wilkins, 2002.

[13] P. Castadot, J.A. Lee, A. Parraga, X. Geets, B. Macq, and V. Grégoire. Comparison of 12 deformable registration strategies in adaptive radiation therapy for the treatment of head and neck tumors. *Radiotherapy and oncology*, 89(1):1–12, 2008.

[14] KS Chao, S. Bhide, H. Chen, J. Asper, S. Bush, G. Franklin, V. Kavadi, V. Liengswangwong, W. Gordon, A. Raben, et al. Reduce in variation and improve efficiency of target volume delineation by a computer-assisted system using a deformable image registration approach. *International Journal of Radiation Oncology* Biology* Physics*, 68(5):1512–1521, 2007.

[15] Z.H. Cho, J.P. Jones, and M. Singh. *Foundations of medical imaging.* Wiley New York:, 1993.

[16] W.R. Crum and DLG Hartkens, T. Hill. Non-rigid image registration theory and practice. *British journal of radiology*, 77(Special Issue 2):S140, 2004.

[17] DAHANCA. Retningslinjer for strålebehandling af hoved-hals cancer, 2004.

[18] T.F. De Laney and H.M. Kooy. *Proton and charged particle radiotherapy.* Lippincott Williams & Wilkins, 2007.

[19] L.R. Dice. Measures of the amount of ecologic association between species. *Ecology*, 26(3):297–302, 1945.

[20] G.X. Ding, D.M. Duggan, C.W. Coffey, M. Deeley, D.E. Hallahan, A. Cmelak, and A. Malcom. A study on adaptive IMRT treatment planning using kV cone-beam CT. *Radiotherapy and oncology*, 85(1):116–125, 2007.

[21] MN Duma, S. Kampfer, T. Schuster, C. Winkler, and H. Geinitz. Adaptive radiotherapy for soft tissue changes during helical tomotherapy for head and neck cancer. *Strahlentherapie und Onkologie*, pages 1–5, 2012.

[22] U.V. Elstroem and C. Grau. Adaptive image-guided radiotherapy for head and neck cancer. *Functional Preservation and Quality of Life in Head and Neck Radiotherapy*, pages 183–190, 2009.

[23] U.V. Elstrøm, B.A. Wysocka, L.P. Muren, J.B.B. Petersen, and C. Grau. Daily kv cone-beam CT and deformable image registration as a method for studying dosimetric consequences of anatomic changes in adaptive IMRT of head and neck cancer. *Acta Oncologica*, 49(7):1101–1108, 2010.

[24] L. Feuvret, G. Noel, J.J. Mazeron, and P. Bey. Conformity index: a review. *International Journal of Radiation Oncology* Biology* Physics*, 64(2):333–342, 2006.

[25] GG Hanna, AR Hounsell, and JM O'Sullivan. Geometrical analysis of radiotherapy target volume delineation : a systematic review of reported comparison methods. *Clinical Oncology*, 22(7):515–525, 2010.

[26] E.K. Hansen, M.K. Bucci, J.M. Quivey, V. Weinberg, and P. Xia. Repeat CT imaging and replanning during the course of IMRT for head-and-neck cancer. *International Journal of Radiation Oncology* Biology* Physics*, 64(2):355–362, 2006.

[27] L.B. Harrison, R.B. Sessions, and W.K. Hong. *Head and neck cancer: a multidisciplinary approach*. Lippincott Williams & Wilkins, 2008.

[28] Onkologisk afdeling R Herlev Hospital. Straalebehandling i hoved- og halsområdet.

[29] J. Hou, M. Guerrero, W. Chen, and W.D. D'Souza. Deformable planning CT to cone-beam CT image registration in head-and-neck cancer. *Medical Physics*, 38:2088, 2011.

[30] C.C. Hu, W.T. Huang, C.L. Tsai, J.K. Wu, H.L. Chao, G.M. Huang, C.W. Wang, C.J. Wu, and J.C.H. Cheng. Practically acquired and modified cone-beam computed tomography images for accurate dose calculation in head and neck cancer. *Strahlenterapie and Onkologie*, pages 1–12, 2011.

[31] ICRU. Prescribing, recording, and reporting photon-beam intensity-modulated radiation therapy (IMRT). *Journal of the ICRU Vol 10 No 1 (2010) Report 83*.

[32] F.M. Khan and S. Stathakis. The physics of radiation therapy. *Medical Physics*, 37:1374, 2010.

[33] Rasmus Larsen. 02505 course note - medical image analysis.

[34] X.A. Li. *Adaptive Radiation Therapy*. CRC Press, 2011.

[35] D. MacDonald. *Oral and Maxillofacial Radiology: A Diagnostic Approach*. Wiley-Blackwell, 2011.

[36] P. Mayles, A. Nahum, JC Rosenwald, and N. Papanikolaou. Handbook of radiotherapy physics: Theory and practice. *Medical Physics*, 35:4281, 2008.

[37] I. Miller, J.E. Freund, and R.A. Johnson. *Probability and statistics for engineers*, volume 4. Prentice-Hall Englewood Cliffs, New Jersey, 1965.

[38] AC Miracle and SK Mukherji. Conebeam CT of the head and neck, part 1: physical principles. *American Journal of Neuroradiology*, 30(6):1088–1095, 2009.

[39] EB Podgorsak et al. *Radiation Oncology Physics*.

[40] J.A. Purdy, J.M. Michalski, J. Bradley, S. Vijayakumar, C.A. Perez, and S.H. Levitt. Three-dimensional treatment planning and conformal therapy. *Technical Basis of Radiation Therapy*, pages 179–202, 2006.

[41] C. Reimann, P. Filzmoser, R.G. Garrett, and R. Dutter. *Statistical data analysis explained*. Wiley Online Library, 2009.

[42] J.P. Thirion. Fast non-rigid matching of 3D medical images. 1995.

[43] J.P. Thirion. Image matching as a diffusion process: an analogy with maxwell's demons. *Medical image analysis*, 2(3):243–260, 1998.

[44] S.Y. Tsuji, A. Hwang, V. Weinberg, S.S. Yom, J.M. Quivey, and P. Xia. Dosimetric evaluation of automatic segmentation for adaptive IMRT for head-and-neck cancer. *International Journal of Radiation Oncology* Biology* Physics*, 77(3):707–714, 2010.

[45] U. Ueda, W. Hu, J. Pouliot, J. Quivey, M. Aubin, and J. Chen. The impact of cone-beam computed tomography (CBCT) artifacts on deformable image registration algorithms. *AAPM Annual Meeting Program*, 2010.

[46] A. Van Esch, D.P. Huyskens, C.F. Behrens, E. Samsøe, M. Sjölin, U. Bjelkengren, D. Sjöström, L. Clermont, C. ad Hambach, and F. Sergent. Implementing rapidarc into clinical routine: A comprehensive program from machine qa to tps validation and patient QA. *Medical Physics*, 38:5146, 2011.

[47] Varian. *SmartSegmentation ®Knowledge Based Contouring Reference Guide*, March 2011.

[48] H. Wang, L. Dong, J. O'Daniel, R. Mohan, A.S. Garden, K.K. Ang, D.A. Kuban, M. Bonnen, J.Y. Chang, and R. Cheung. Validation of an accelerated 'demons' algorithm for deformable image registration in radiation therapy. *Physics in Medicine and Biology*, 50:2887, 2005.

[49] E.C. Ward and C.J. van As-Brooks. Head and neck cancer: treatment, rehabilitation, and outcomes. 2007.

[50] Q. Wu, Y. Chi, P.Y. Chen, D.J. Krauss, D. Yan, and A. Martinez. Adaptive replanning strategies accounting for shrinkage in head and neck IMRT. *International Journal of Radiation Oncology* Biology* Physics*, 75(3):924–932, 2009.

[51] Y. Yang, E. Schreibmann, T. Li, C. Wang, and L. Xing. Evaluation of on-board kV cone beam CT (CBCT)-based dose calculation. *Physics in medicine and biology*, 52:685, 2007.